ORNL-3026
UC-80 - Reactors - General

BURNOUT HEAT FLUXES FOR LOW-PRESSURE WATER IN NATURAL CIRCULATION

W. R. Gambill
R. D. Bundy

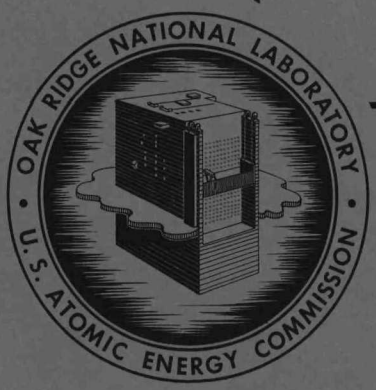

OAK RIDGE NATIONAL LABORATORY
operated by
UNION CARBIDE CORPORATION
for the
U.S. ATOMIC ENERGY COMMISSION

DISCLAIMER

ORNL-3026

Contract No. W-7405-eng-26

REACTOR DIVISION

BURNOUT HEAT FLUXES FOR LOW-PRESSURE WATER IN NATURAL CIRCULATION

W. R. Gambill

R. D. Bundy

DATE ISSUED

DEC 2 0 1960

OAK RIDGE NATIONAL LABORATORY
Oak Ridge, Tennessee
Operated by
UNION CARBIDE CORPORATION
for the
U. S. ATOMIC ENERGY COMMISSION

BURNOUT HEAT FLUXES FOR LOW-PRESSURE WATER IN NATURAL CIRCULATION

W. R. Gambill
R. D. Bundy

ABSTRACT

Twenty-nine experimental determinations of burnout heat flux were made with water flowing by natural circulation through electrically heated vertical tubes with and without internal twisted tapes and through rectangular cross sections of three aspect ratios. Heated lengths varied from 10 to 33 in., system pressure at the test-section flow exit from 14.7 to 26.3 psia, inlet subcooling from 36 to 170°F, and burnout heat flux from 13,000 to 218,500 Btu/hr·ft^2. Tests were made with both unrestricted and restricted return flow paths.

Three correlations were developed for predicting natural-circulation burnout heat fluxes for such conditions. Two are useful for rapid estimation, but the third involves a more fundamental assessment of the coolant mass velocity at burnout by a graphical matching of the heat flux which a given flow rate can sustain to the heat flux which will produce that flow rate. For all the data, this approach gave average and maximum deviations of 15% and 38%, respectively. It has been found that use of a slip ratio of unity is adequate for burnout prediction, and the reasons for this are discussed in detail. The small burnout penalty incurred by a substantial restriction of return flow path, experimentally observed, is in complete accord with the theoretical model.

CONTENTS

INTRODUCTION

Scope

The experimental program was initially oriented toward determination of burnout heat fluxes and surface temperature distributions for the parallel-plate core of the High Flux Isotope Reactor during various stages of the core-removal sequence, when heat is removed by natural circulation alone. Toward this end, a series of tests was conducted with resistance-heated rectangular test sections and environmental conditions approximating those anticipated during HFIR core removal. Similar data were later obtained for the Oak Ridge Research Reactor coolant-channel geometry. The natural-circulation experimental program was extended finally to other coolant-channel geometries, including empty tubes and tubes with full-length internal twisted-tape swirl generators.

Natural Circulation and the Causes of Burnout During Natural Circulation

When a channel immersed in liquid is heated, the density of the liquid within the channel decreases as its temperature increases. The difference between the density of the liquid within the channel and the density of the unheated liquid outside causes an upward flow of coolant through the heated channel.

The coolant flow rate is always such that the pressure losses resulting from flow through the channel (entrance, exit, frictional, and acceleration losses) and through some return path balance the driving pressure arising from the difference in density. Figure 1 shows a typical heat flux versus flow rate relationship for natural circulation from the data of Rathbun, Van Huff, and Weiss.[1]

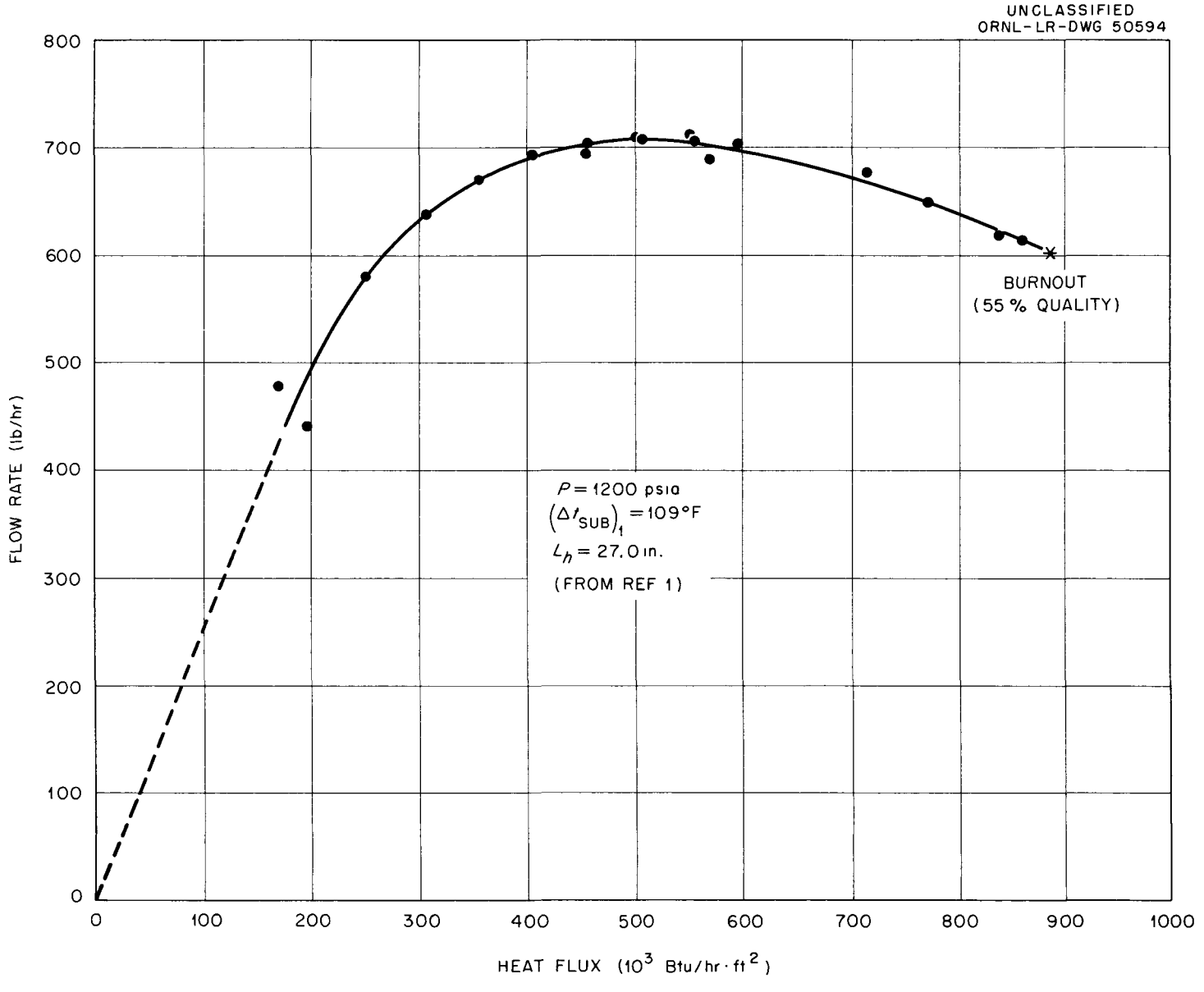

Fig. 1. Heat Flux vs Coolant Flow Rate for a 0.210 in x 2.00 in Channel.

As the heat flux in the channel is increased, the increasing density difference between the fluid outside and inside the channel increases the flow rate through the channel. At some heat flux, the temperature of the fluid at the channel exit reaches the local boiling point. The high linear exit velocities resulting from the low mixture densities corresponding to net vaporization cause the acceleration loss to increase, and the flow rate through the channel increases more slowly with increasing heat flux after net vaporization begins. Further increases of applied heat flux cause the point at which boiling occurs to move down the channel, and the mean fluid density in the channel decreases. The increased acceleration and frictional losses within the heated channel, however, more than offset the increased driving force, and the flow rate reaches a maximum at small vapor qualities.

As the heat flux is increased further, a critical or burnout heat flux is reached. At this point, the channel can no longer be cooled effectively by natural circulation; and if the heat flux is independent of the heat-transfer characteristics of the coolant flow, as with electrical or nuclear heating, wall temperatures rise rapidly and the channel "burns out". A critical heat flux may be reached in three ways; Fig. 2 is a diagram of the conditions preceding each of the possible burnout mechanisms.

Figure 2a shows the most common mode of burnout. The maximum heat flux which can be sustained in a given channel during bulk boiling is proportional to the mass velocity to some power. As the applied heat flux in the channel is increased, the eventual decrease in flow rate decreases the maximum heat flux which can be sustained. Finally, film boiling begins when a heat flux is reached at which the flow rate can no longer support the maximum applied heat flux.

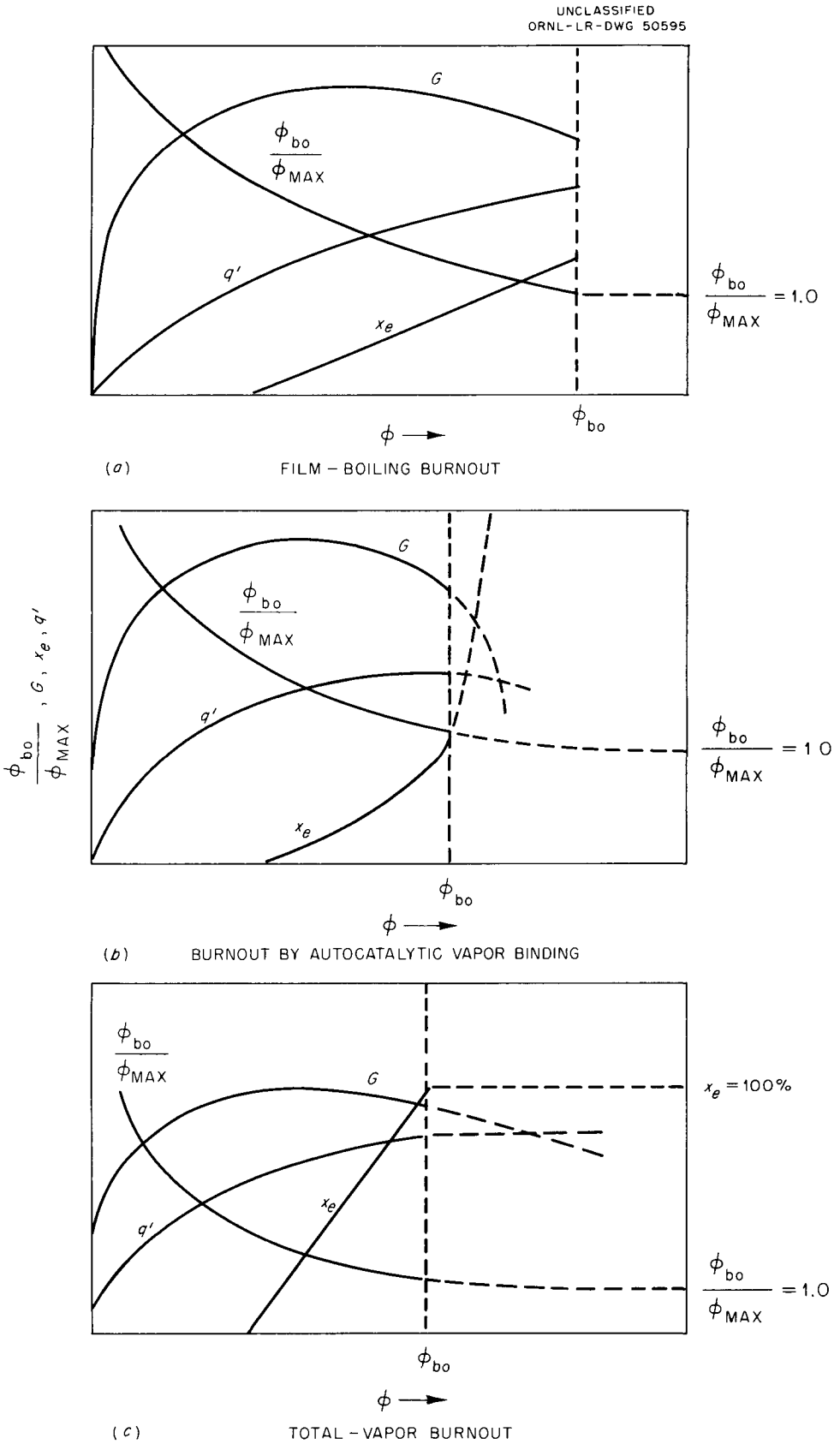

Fig. 2. Modes of Natural - Circulation Burnout.

Figure 2b represents the case where the mass velocity decreases very rapidly with increasing vapor quality. The mass velocity decreases so rapidly that there is a maximum amount of heat (product of flow rate and enthalpy change) which can be removed by the coolant. When more heat than this is delivered to the coolant, the vapor quality rises rapidly; the mass flow rate and heat removal drop even more; and the heated channel "vapor locks" before film-boiling burnout correlations indicate that the critical heat flux has been reached.

Figure 2c represents the case in which exit vapor quality smoothly attains 100% before film-boiling correlations indicate that burnout should have occurred. Even with flow in a regime which is characterized by a continuous vapor phase, relatively high heat fluxes may be sustained by liquid boiling at the wall. Goldmann, Firstenberg, and Lombardi[2] discuss the method by which liquid droplets diffuse toward the wall because of the concentration gradient caused by the evaporation at the wall. When the vapor quality approaches 100%, sufficient droplets to maintain as high a heat flux as before are no longer available. Isbin[3] observed a marked decrease in the heat-transfer coefficient between 99% and 100% vapor quality. In Fig. 2c the heat flux is small enough to be removed by the evaporating liquid droplets ($\phi_{bo}/\phi_{max} > 1.0$), but is too large to be sustained by heat transfer to vapor, and the channel burns out at essentially 100% quality. Calculated qualities for several tests of the present study reached 100% at the exit (see Table 1-b). Burnout heat fluxes calculated on the basis of burnout at 100% quality for these tests agree well with the experimental values. Each of these three methods of burnout exhibits a critical dependence on mass flow rate.

Pressures, flow rates, and bulk and wall temperatures may fluctuate about their mean values during natural circulation. If these fluctuations are severe, burnout may occur prematurely. Film boiling may begin at the minimum of a flow oscillation. If the heat flux is large enough, compared to the heat capacity, burnout will occur before the flow recovers. Also, the reduction of flow during an oscillation produces a corresponding increase in vapor quality. If conditions are such that an increase in quality can decrease the ability of the coolant to remove heat (see right end of q' curve of Fig. 2b), the flow will not recover and the channel will burn out by "vapor binding".

Two-Phase Flow

At burnout in a channel cooled by natural circulation of low-pressure water, two-phase flow exists. Therefore some knowledge of vertical two-phase flow is needed to fully understand natural-circulation burnout. A brief discussion of some aspects of two-phase flow follows.

Govier, Radford, and Dunn[4] made visual observations of the dispersion of air and water during vertical two-phase flow. They found that the vapor is dispersed as bubbles in the liquid at very small vapor fractions. As the vapor fraction increases, the bubbles collect into slugs of vapor, which travel at a higher velocity than the liquid. A frothy flow of liquid and vapor replaces slug flow at still higher vapor qualities; next, frothy flow is replaced by an annular flow of liquid around a central core of vapor traveling at a higher velocity. Finally, at very high vapor fractions, annular flow collapses into a mist or fog of liquid droplets suspended in vapor. The results of Govier and co-workers are in general agreement with those of other observers.

Lockhart and Martinelli[5] classified two-phase flow of air and water according to whether the separate liquid and vapor flows were viscous or turbulent. Their correlations show that the frictional pressure drop for two-phase flow is much larger than that calculated using a homogeneous model (intimate mixing of liquid and vapor with no net difference in their velocities) and that the mixture density in two-phase flow is greater than that calculated from a homogeneous model.

Martinelli and Nelson[6] modified the correlation of Lockhart and Martinelli[5] for boiling water. They also correlated the acceleration loss for the flow of boiling water.

Govier, Radford, and Dunn[4] observed four flow regimes, with a different pressure-drop behavior in each, for the isothermal two-phase flow of air and water. The extent of these regimes and the flow behavior within them was found to depend on the liquid velocity, the volume ratio of vapor to liquid, (and from later studies[7,8]) the channel diameter and the pressure.

Alves[9] concluded from studies with 1-in. pipes that the type of flow should be known when estimating two-phase pressure drops with the Lockhart-Martinelli correlation. Baker[10] cites other data to show that the turbulent-turbulent data of Lockhart and Martinelli[5] apply primarily to annular flow. Isbin and co-workers[11] report that the Martinelli correlations overpredict their experimental pressure drops.

The experiments of Govier and Short[7] and of Bailey and associates[12] show that the effect of slip decreases at smaller tube diameters. The data of the present study seem to indicate that the effect of slip on burnout is very small for flow channels having equivalent diameters less than 1/4 in.

During bulk-boiling natural circulation, the coolant probably passes through several pressure drop, flow, and turbulence regimes as it moves up the heated channel. The flow regimes encountered during natural-circulation bulk boiling and the conditions for transition from one to another are not presently well understood. The effect of flow conditions on slip are also not known for all flow regimes. Many of the available data were taken with horizontal tubes and are not necessarily applicable to vertical two-phase flow. These factors combine to make the effect of slip on density and pressure drop during natural circulation extremely difficult to assess.

EXPERIMENTAL PROGRAM

System Description

The experimental system used in this study is depicted schematically in Fig. 3. Rectangular test sections were fabricated by welding A-nickel plates over Inconel spacer strips; the nickel plates were reduced in thickness at the edges which overlapped the Inconel strips in order to reduce heat generation in the metal at the sides of the flow channel. Figure 4 is the cross section of a typical rectangular test section. Copper tubes with full-length internal twisted tapes were produced by twisting Inconel strips (while loaded axially to about 20,000 psi) so that the twisted tapes would slip easily into the copper tube, and then drawing the tubes down onto the tapes until the tape edges penetrated the tube wall about 1 mil. Empty copper tubes were also tested. The dimensions of all test section are given in Table 1-a.

The system was filled with distilled water of the desired temperature from a fill line above the system. During the tests, coolant entered the

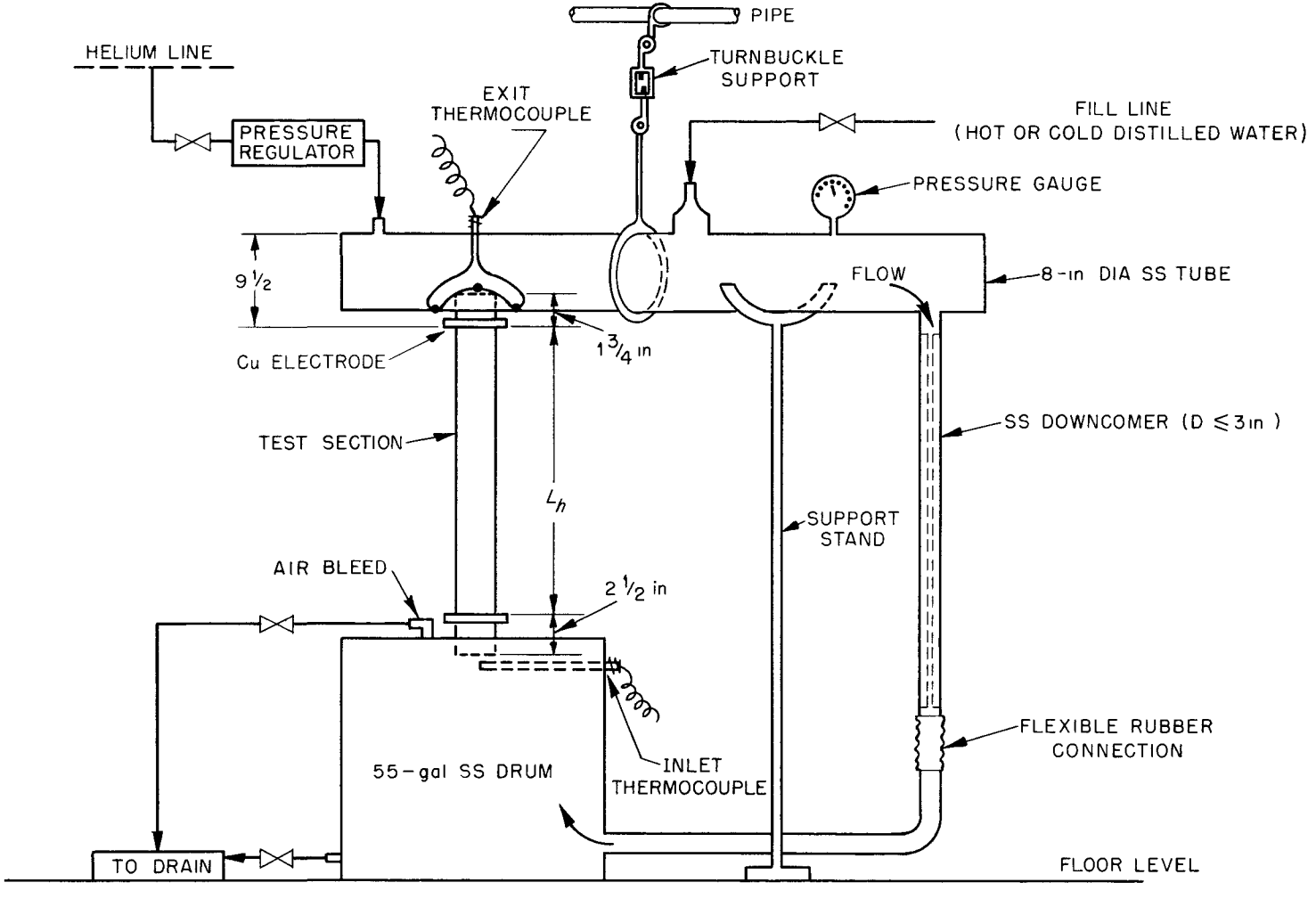

Fig. 3. Experimental System for Natural-Circulation Heat Transfer Tests.

UNCLASSIFIED
ORNL-LR-DWG 50597

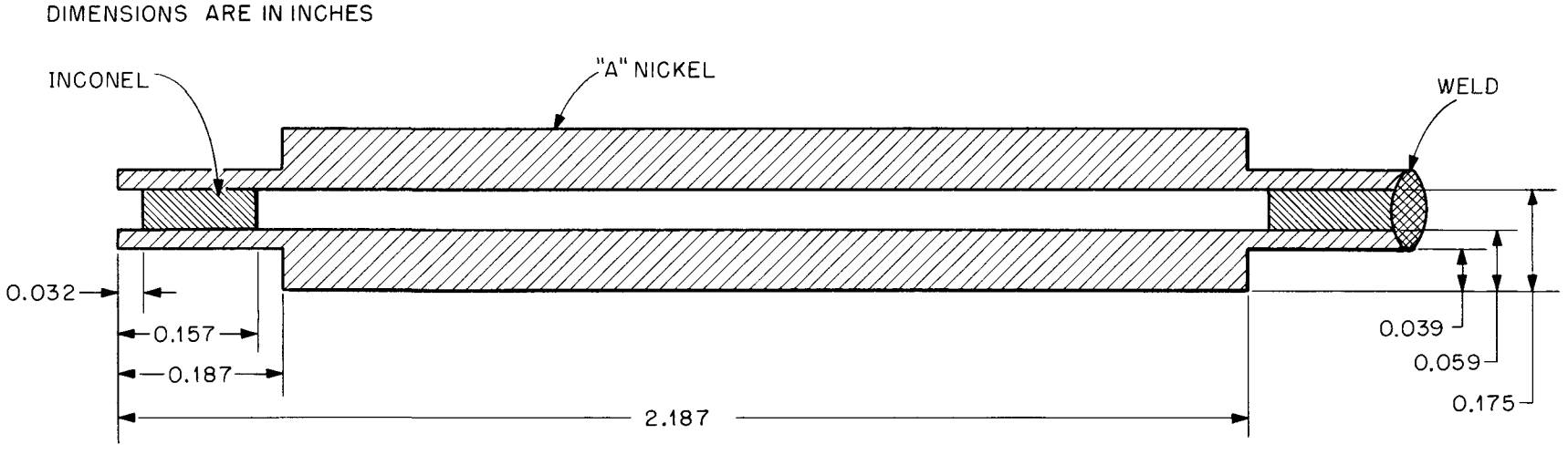

Fig. 4. Cross-Sectional View of Typical Rectangular Test Section.

Table 1-a. Natural-Circulation Burnout Data

Test No.	Test Conditions: Flow Channel Dimensions (in.)	L_h (in.)	L_t (in.)	y (dia/180-deg twist)	Material	P_2[a] (psia)	t_{b_1} (°F)	$(\Delta t_{sub})_1$ (°F)	Downcomer ID (in.)	A_{TS}/A_D[b]
1	0.056 x 1.06	17.99	22.0	---	0.057 A-nickel	20.2	75 - 77	151	2.870	0.0092
2	0.053 x 1.06	17.94	22.0	---	separated by	15.4	68 - 75	140	2.870	0.0087
3	0.052 x 1.08	17.80	22.0	---	0.050 Inconel	25.7	122 - 125	117	2.870	0.0087
4	0.054 x 1.06	17.94	22.0	---	spacers	20.6	75	154	2.870	0.0088
5	0.052 x 1.11	17.92	22.0	---	"	25.7	124 - 128	114	0.000	∞
6	0.052 x 1.06	17.92	22.0	---	"	25.7	124	118	0.137	3.72
7	0.052 x 1.06	17.92	22.0	---	"	25.2	122	119	0.095	7.65
8	0.052 x 1.06	17.92	22.0	---	"	25.0	123	117	0.000	∞
9	0.116 x 2.07	23.38	27.0	---	0.059 A-nickel	25.5	121	120	0.000	∞
10	0.119 x 2.07	23.33	27.0	---	separated by	20.0	86	142	2.870	0.0381
11	0.119 x 2.07	23.33	27.0	---	0.116 Inconel spacers	26.3	127	116	2.870	0.0381
12	0.119 x 2.07	23.33	27.0	---	"	15.0	129	84	2.870	0.0381
13	0.113 x 2.09	23.65	35.5	---	0.057 A-nickel	26.1	115	127	0.180	8.86
14	0.066 x 2.26	33.28	37.0	---	separated by	24.5	176	63	2.870	0.0231
15	0.066 x 2.26	33.28	37.0	---	0.060 Inconel spacers	15.8	78	137	2.870	0.0231
16	0.066 x 2.26	33.28	37.0	---	"	14.7	176	46	2.870	0.0231
17	0.066 x 2.26	33.28	37.0	---	"	15.2*	184	40	2.870	0.0231
18	0.066 x 2.26	33.28	37.0	---	"	14.7	84	138	2.870	0.0231
19	0.249 ID	9.99	14 0	---	0.249 x 0.354	15.0	74	149	2.870	0.0076
20	0.249 ID	10.05	14.0	---	copper tubes	25.0	76 - 78	162	2.870	0.0076
21	0.249 ID	10.09	14.0	---	"	24.5	169 - 174	65	2.870	0.0076
22	0.249 ID	10.00	13.5	2.30	0.249 x 0.354	24.7	71 - 73	166	2.870	0.0070
23	0.249 ID	10.09	13.5	2.30	copper tubes	15.0	71 - 73	140	2.870	0.0070
24	0.249 ID	10.06	13.5	4.94	with full-length	15.0	78	135	2.870	0.0070
25	0.249 ID	10.09	13.5	8.03	0.015 Inconel twisted tapes	15.0	82	131	2.870	0.0070
26	0.249 ID	10.09	13.5	4.94	"	24.6	64	175	2.870	0.0070
27	0.249 ID	10.08	13.5	4.94	"	24.8	177 - 180	59	2.870	0.0070
28	0.249 ID	10.12	13.5	8.03	"	24.8	69	170	2.870	0.0070
29	0.249 ID	10.12	13.5	8.03	"	25.1	176 - 179	61	2.870	0.0070

[a] Pressure at top of heated length of test section.

[b] Ratio of the test-section coolant-flow area to that of a section of the downcomer having the same total length as the test section. The rest of the downcomer had a coolant-flow area much larger than that of the test section.

* At burnout, the liquid level was 10-3/4 in. below the heated exit.

Table 1-b. Natural-Circulation Burnout Data

Test No.	$(x_e)_{bo}$[c] Calculated (%)	$(t_i)_{max}$[d] (°F)	$(\phi_{bo})_{exptl}$[e] (Btu/hr·ft²)	$(\phi_{bo})_{pred}$[f] (Btu/hr·ft²)	$(\phi_{bo})_{exptl}/(\phi_{bo})_{pred}$
		Test Results			
1	96	232	48,800	68,000	0.718
2	100	214	52,200	63,600	0.833
3	98	433	83,100	83,000	1.001
4	99	226	50,100	71,500	0.700
5	--	293	13,000	---	---
6	97	277	70,600	78,000	0.905
7	100	260	61,500	69,500	0.885
8	--	402	19,700	---	---
9	--	242	18,500	---	---
10	82	244	127,100	122,000	1.043
11	76	266	127,100	136,000	0.930
12	77	--	95,200	111,000	0.863
13	27	254	151,400[g]	153,000	0.990
14	100	286	67,700	63,500	1.066
15	100	225	59,300	57,100	1.039
16	100	239	51,100	49,400	1.034
17	100	232	49,000	43,400	1.114
18	100	221	30,500	39,600	0.770
19	80	259	118,900	137,000	0.868
20	75	271	137,100	166,000	0.826
21	85	246	218,500	158,000	1.383
22	100	273	144,200	164,000	0.879
23	100	257	135,500	144,000	0.941
24	97	246	114,700	156,000	0.735
25	80	239	126,900	167,000	0.760
26	75	248	139,100	196,000	0.710
27	89	228	198,900	188,000	1.058
28	73	259	143,900	205,000	0.702
29	84	255	175,900	193,000	0.911

[c] Exit quality calculated from the semitheoretical burnout prediction method presented in this report (homogeneous flow model).

[d] Defined as the maximum surface temperature reached just before the sharp rise in temperature at burnout.

[e] Corrected from an average to a maximum value by using the electrical resistivities corresponding to the measured maximum and average wall temperatures.

[f] Predicted using the semitheoretical burnout prediction method presented in this report (homogeneous flow model).

[g] $\phi_{max}/\phi_{avg} = 2.19$.

test section from a 55-gal stainless steel storage drum. Water flowed from the test section into an 8-in.-dia stainless steel header. The return path for flow was of 3-in. stainless steel tubing. The volume of the system was sufficiently large that the inlet water temperature remained very nearly constant for the duration of most of the tests. Regulated helium was used to pressurize the entire system to the desired operating level.

The test sections were resistance heated with 60-cycle alternating current. One-inch-thick copper electrodes were silver soldered to the ends of the test section and connected to a power transformer by leaf extensions or by multiple 300 amp cables. The leaf extensions were composed of interleaved copper plates 4 in. wide and 3/8 in. thick. The superficial contact area at the intermediate press fits was double the cross-sectional area of the plates. The maximum connector and electrode current density attained during the tests was about 2500 amp/in.^{2} The heat generation was determined by the product of the voltage across the test section and the current through it. The current was reduced with a current transformer and read on a calibrated ammeter. The voltage, read on a calibrated voltmeter, was corrected to the voltage across the test section by multiplying by the ratio of heated to voltage-tap length. The power factor, measured with a phase-angle meter for the test section used in tests 10 through 12, was 0.97. This correction was applied to all the tests. The calculated heat generation in the edges of the rectangular test section ($\sim$ 7%) was subtracted from the total heat generation to obtain the heat generated in the flat plates being tested. Calculated external radiant and convective heat losses were subtracted from the electrical input to obtain the heat passing into the coolant. Heat fluxes were further corrected from an average to a maximum value using the electrical

resistivity values corresponding to the measured average and maximum wall temperatures.

The inlet water temperature was obtained from a thermocouple probe placed directly beneath the test section. The exit water temperature was measured with a thermocouple bead positioned in the center of the flow-channel exit by the lead wires, which were stretched across the top of the test section and insulated from it. Outside surface temperatures were measured by Chromel-Alumel thermocouples discharge welded to the outside of the test sections. The test sections were thermally insulated with 1 to 2 in. of Fiberfrax.

Because of the low heat fluxes, the burnout process occurred relatively slowly during the natural-circulation tests; and, when desired, burnout could be avoided by quickly decreasing the voltage across the test section. In this manner, several burnout determinations could be made with a single test section. When the metal temperature increased sharply at the beginning of burnout, the increased electrical resistance caused the observed voltage to increase and the current to decrease; the maximum value of observed current was used as the burnout criterion and for calculating the burnout heat flux. Maximum temperatures (or metal failure) occurred at the top of the test section when the coolant was externally recirculated, and at the bottom of the section when no return leg was used.

Ranges of Conditions

Twenty-nine experimental determinations of burnout heat flux were made. Heated length was varied from 10 to 33 in., equivalent diameter from 0.10 to 0.25 in., system pressure at the test-section exit from 14.7 to 26.3 psia, and inlet subcooling from 36 to 170°F. Corrected burnout heat fluxes varied

from 13,000 to 218,500 Btu/hr·ft^2. The conditions for each test are listed in Table 1-a.

The water resistivity ranged from 37,500 to 305,000 ohm-cm except for one sample (test 21), which read 8000 ohm-cm. The average water resistivity was 149,000 ohm-cm. Resistivities were measured for water samples at temperatures from 21 to 31.5°C. The pH of the coolant water ranged from 6.18 to 7.95 (6.66 average).

EXPERIMENTAL RESULTS

Burnout Heat Fluxes

Table 1-b gives the experimentally determined burnout heat flux for each test. In tests 1 and 4 the burnout heat flux was obtained for conditions which simulate those encountered when the HFIR core just clears the top of the pressure vessel during core removal. Test 3 corresponds to conditions when the HFIR core has just been lifted from the core grid within the pressure vessel. Tests 5 through 8 were conducted to investigate the effect on natural-circulation burnout heat flux of different restrictions to external recirculation, in simulation of the HFIR core while still on the support grid. In tests 5 and 8 external recirculation was completely prevented by stoppers placed in the return leg. The burnout heat fluxes obtained were 13,000 and 19,700 Btu/hr·ft^2 or 15.6% and 23.7%, respectively, of the value of 83,100 Btu/hr·ft^2 obtained in test 3 for burnout under similar conditions but with unrestricted external recirculation. In tests 6 and 7 a section of the large downcomer was replaced with tubing having the same length as the total length of the test section, but with less flow area. The ratio of test-section flow area to downcomer flow area is listed in Table 1-a for

all tests. The results of these tests are plotted in Fig. 5. The dependence of burnout heat flux on relative flow area in the return leg may be expressed by:

$$\phi_{bo} = 13{,}000 + \frac{1.22 \times 10^6}{17.4 + \left(\frac{A_{TS}}{A_D} \right)} \qquad (1)$$

if the unheated length for which the flow is restricted is about the same as the length of the test section.

Tests 9 through 13 were conducted to determine the burnout flux for natural circulation under various conditions for the Oak Ridge Research Reactor coolant-channel geometry. With conditions similar to those in the ORR after core shutdown, but with unrestricted external recircualtion in test 11, the burnout heat flux was 127,100 Btu/hr·ft^2. With similar conditions, but with external recirculation completely prevented in test 9, the burnout flux was 18,500 Btu/hr·ft^2, or 14.6% of the value with unrestricted external recirculation. Test 13 was conducted with conditions as similar as possible to those in the ORR after shutdown. The ratio of maximum to average heat flux was 2.19. Unheated 6-in. extensions of the coolant channel on each end of the heated length simulated end boxes. A section of the downcomer (same length as the test section) was restricted to 11.3% of the flow area of the test section. The observed maximum and average burnout heat fluxes were 151,400 and 69,100 Btu/hr·ft^2, respectively. The high value of maximum heat flux results from the maximum in the flow rate versus heat flux relationship shown in Fig. 1. The large ratio of maximum to average heat flux causes burnout to occur at a lower average heat flux. The mass velocity is greater at the lower average heat flux, however,

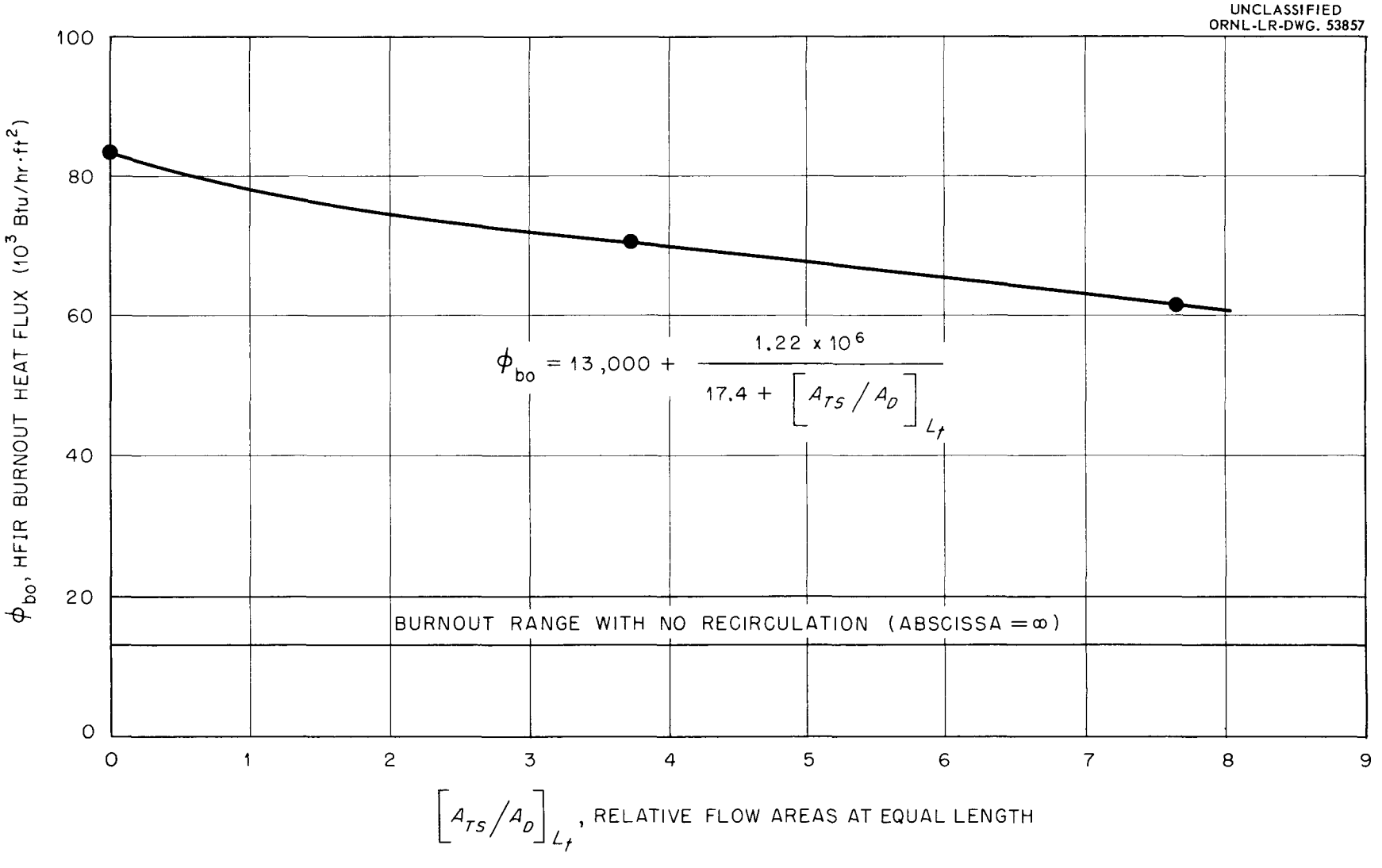

Fig. 5. Variation of HFIR Burnout Heat Flux with Downcomer Flow Area.

and the maximum heat flux which can be sustained is greater.

Surface Temperatures

Measured outside surface temperatures were corrected to inside surface temperatures by using:

$$\Delta t_w = \frac{\phi x}{2 k} \quad . \qquad (2)$$

In none of the tests did the temperature drop across the wall exceed a few degrees Fahrenheit.

Inside surface temperatures increased rapidly from the inlet bulk coolant temperature with no heating to slightly above the coolant saturation temperature at very low heat fluxes. The surface temperatures leveled off just above the saturation temperature and remained nearly constant with increasing heat flux until they rose sharply at burnout. The maximum operating surface temperature, defined as the maximum measured surface temperature (corrected to the inner surface) attained before the sudden rise at burnout, is tabulated as $(t_i)_{max}$ for each test in Table 1-b. Figure 6 gives the maximum inside surface temperature as a function of heat flux for tests 1 through 8, which correspond to the HFIR coolant geometry. The maximum inside surface temperature for tests 9 through 13 (ORR coolant geometry) are given as a function of heat flux in Fig. 7.

Flow Oscillations

In about half the tests, the initial applied heat flux was small enough to allow observation of the beginning of a fluctuation of exit water temperature, which invariably occurred as the heat generation was increased. The observed temperature oscillations, tabulated in Table 2, doubtless arise from changes of the coolant flow rate since the heat flux was constant during any

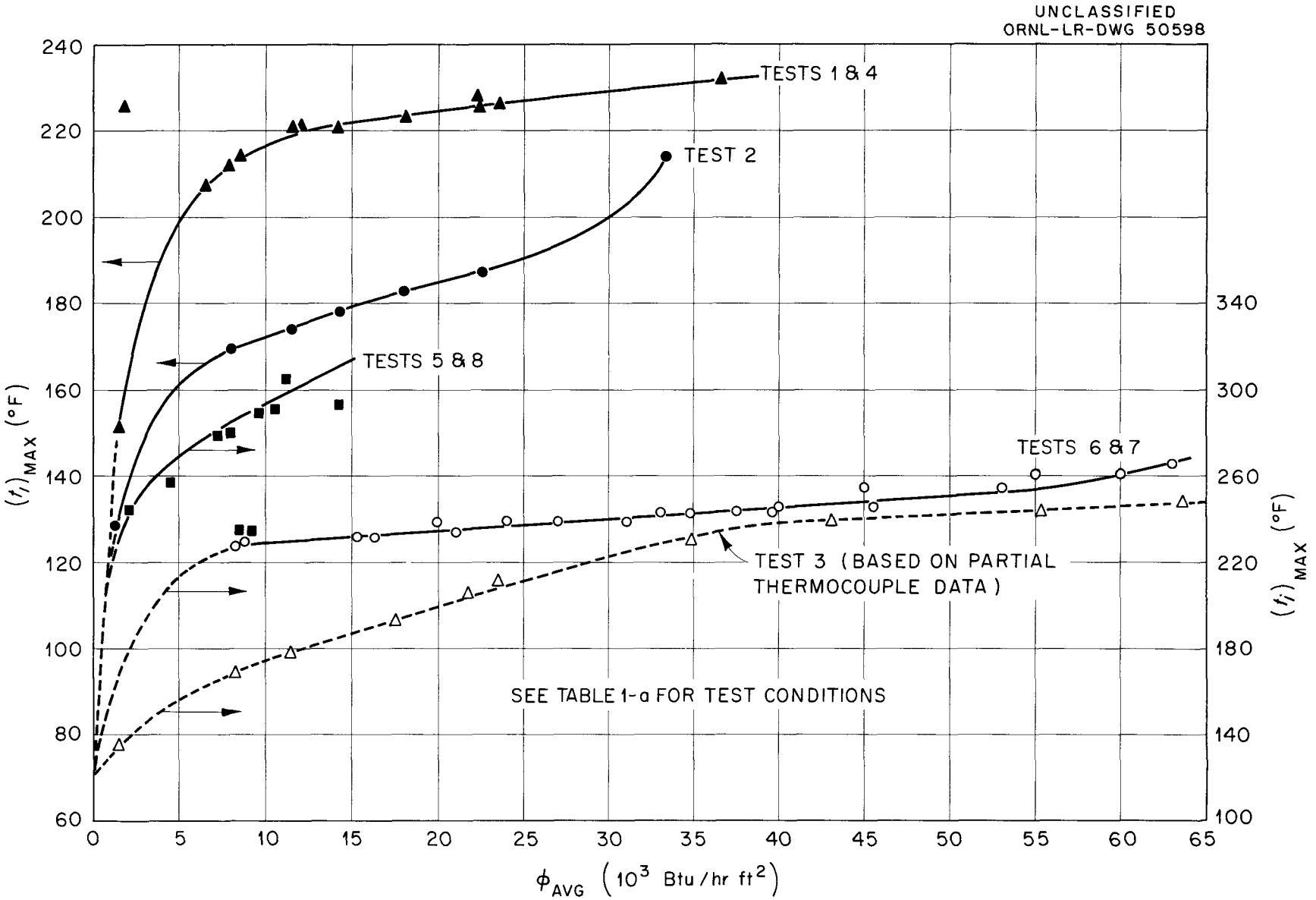

Fig. 6. HFIR Natural-Circulation Heat-Transfer Tests. Maximum Inner Surface Temperature vs Heat Flux.

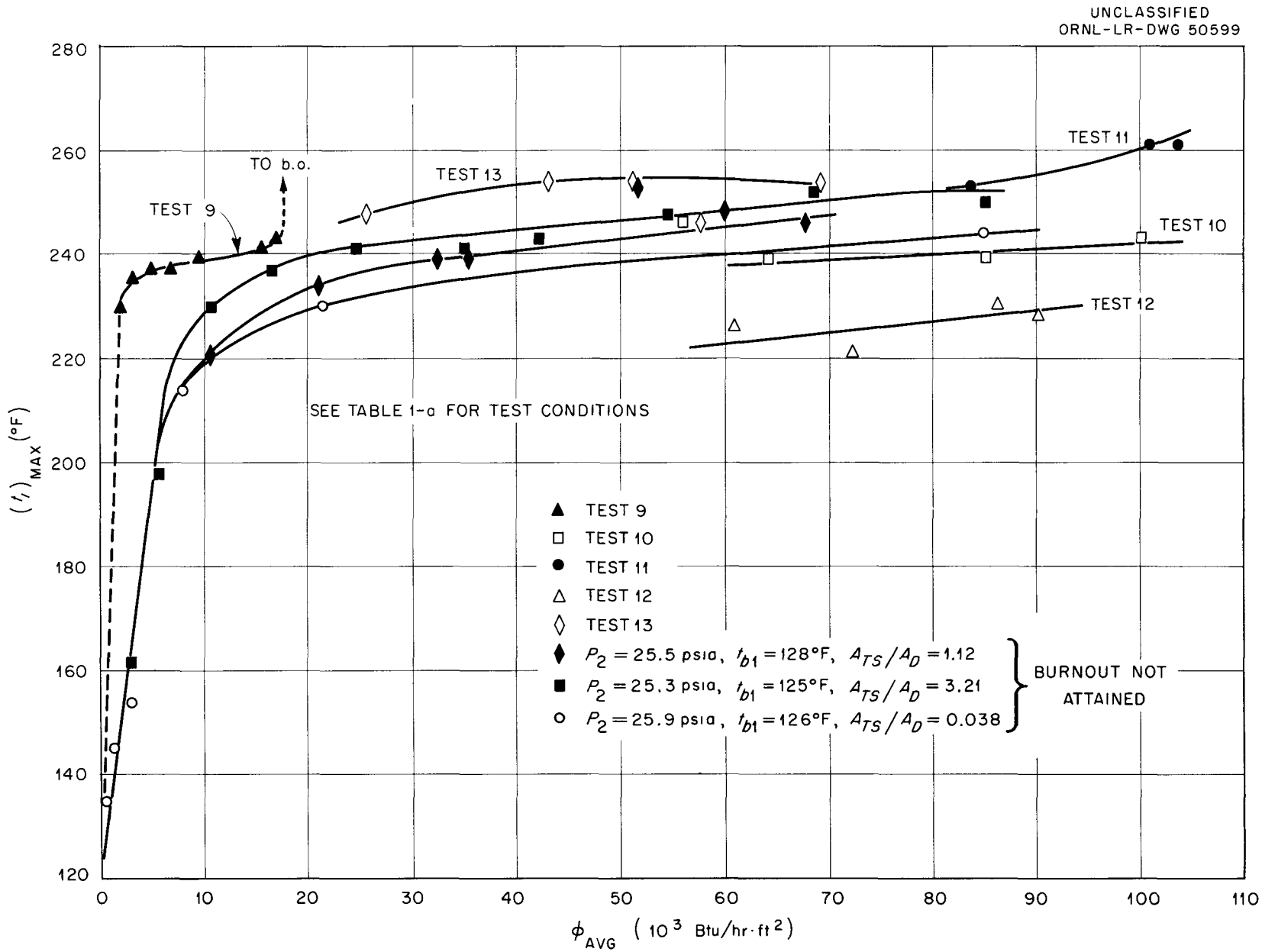

Fig. 7. Maximum Inner Surface Temperature vs Heat Flux for ORR Natural-Circulation Heat-Transfer Tests.

Table 2. Heat Flux Thresholds for Flow Oscillation

Test No.	Lower[a] (Btu/hr·ft^2)	Upper[b] (Btu/hr·ft^2)
1	1,700	11,700
2	1,540	11,400
3	---	10,600
4	1,800	13,200
5	---	5,200
9	2,140	---
20	94,000	---
21	33,900	54,400
22	52,500	63,500
23	---	68,600
24	---	62,300
25	---	95,500
26	77,000	---
27	74,600	---

[a]The heat flux at which the exit water temperature began a stable oscillation of low frequency (<1 cps) and small amplitude (±9 to 15°C maximum).

[b]The heat flux at which the exit water temperature began a stable oscillation of higher frequency (>1 cps) and larger amplitude (±19 to 25°C maximum).

measurement period. It is possible that the frequency of oscillation is related to the natural oscillation frequency of the fluid in the loop. Wall surface temperatures drifted mildly about their average level during this range of operation, but the observed variation was always small relative to that of the exit water temperature. Recent studies of flow oscillations in heated channels have been summarized in papers by Quandt[13] and by Levy and Beckjord.[14]

CORRELATION OF RESULTS

Method of Lee, Dorsey, Moore, and Mayfield

Lee, Dorsey, Moore, and Mayfield[15] have studied the effect of pressure and channel length on maximum heat flux for a variety of fluids flowing in 0.834-in.-ID tubes. The conditions of their tests with water as coolant are summarized in Table 3. These experimenters found that they could correlate their data using the dimensional groups:

$$X = \left(\frac{\rho_\ell - \rho_v}{\rho_v} \right) \left(\frac{1}{\sigma C_{p,\ell}} \right) \left(\frac{L_h}{10} \right)^{0.5} \tag{3}$$

and

$$Y = \frac{\phi_{bo} (\Delta H_{fg}) M_v}{\sigma (t + 460)^2} \left(Pr \right)_\ell^{-0.5} \left(\frac{L_h}{10} \right)^{0.5} , \tag{4}$$

where the relationship between X and Y is shown as Fig. 8.

The equivalent diameter was constant in the tests of Lee and associates, and their correlation does not attempt to account for the effect of this parameter on maximum heat flux. Figure 9 is a plot of the ratio of the experimental to predicted burnout heat flux versus D_e, both for the data of

Table 3. Data of Lee, Dorsey, Moore, and Mayfield[15] for Burnout of 0.834-in.-ID Tubes Cooled by Water in Natural Circulation

$$\left[(\Delta t_{sub})_l = 0\right]$$

Test No.	P (psia)	L (ft)	ϕ_{bo}[a] (10^3 Btu/hr·ft^2)
1	127	10	78.0
2	67	10	102.5
3	14.7	10	54.8
4	3.7	10	26.0
26	127	5	98.0
27	67	5	158.0
28	14.7	5	93.0

[a]These values correspond to peak heat fluxes taken as the maxima of experimentally determined $\phi - \Delta t_f$ curves. Actual burnout did not occur since condensing steam was the heat source.

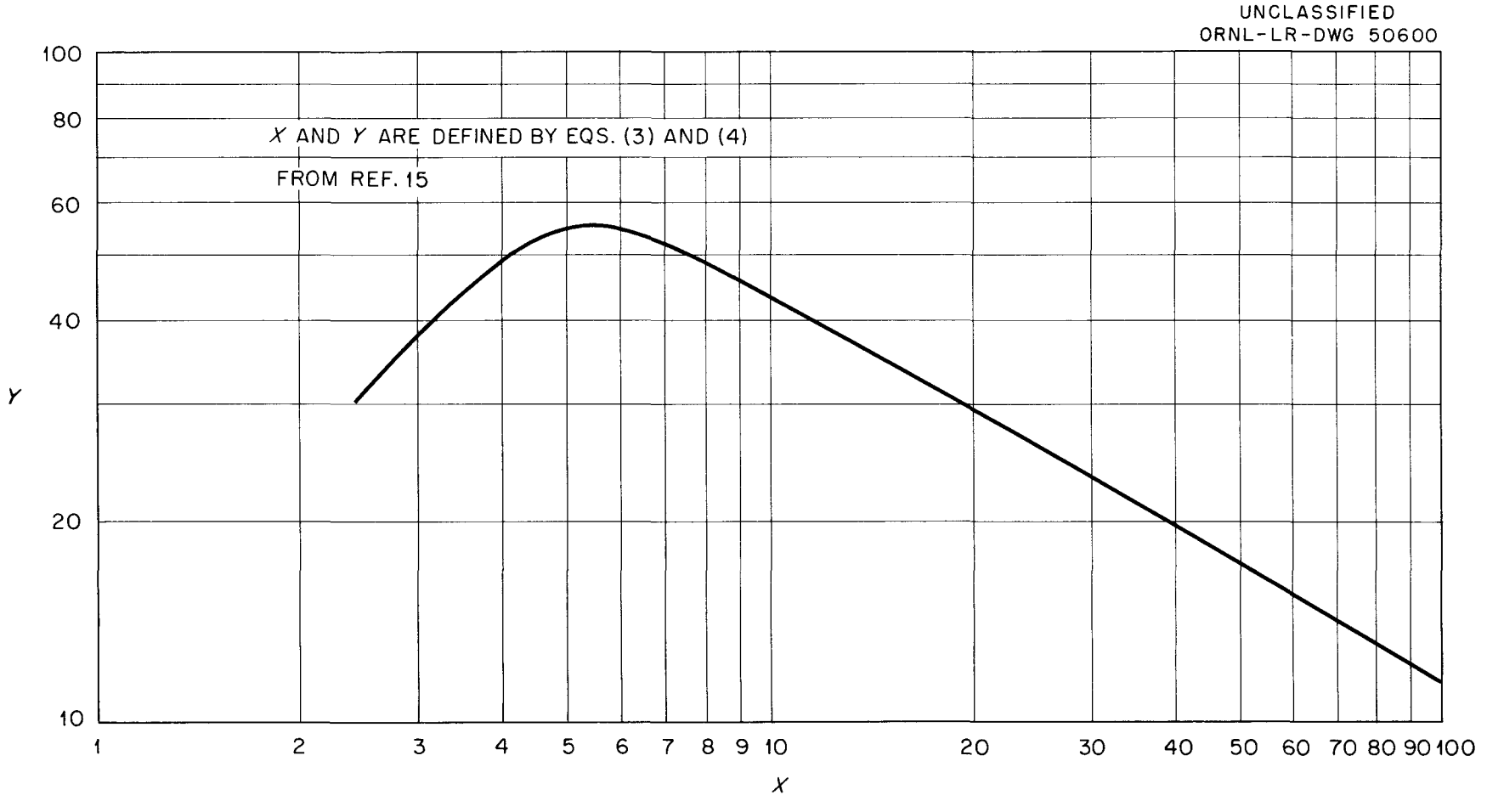

Fig. 8. Correlation of Lee *et al*, for Maximum Heat Flux in 0.83-in. ID Tubes Cooled by Natural Circulation.

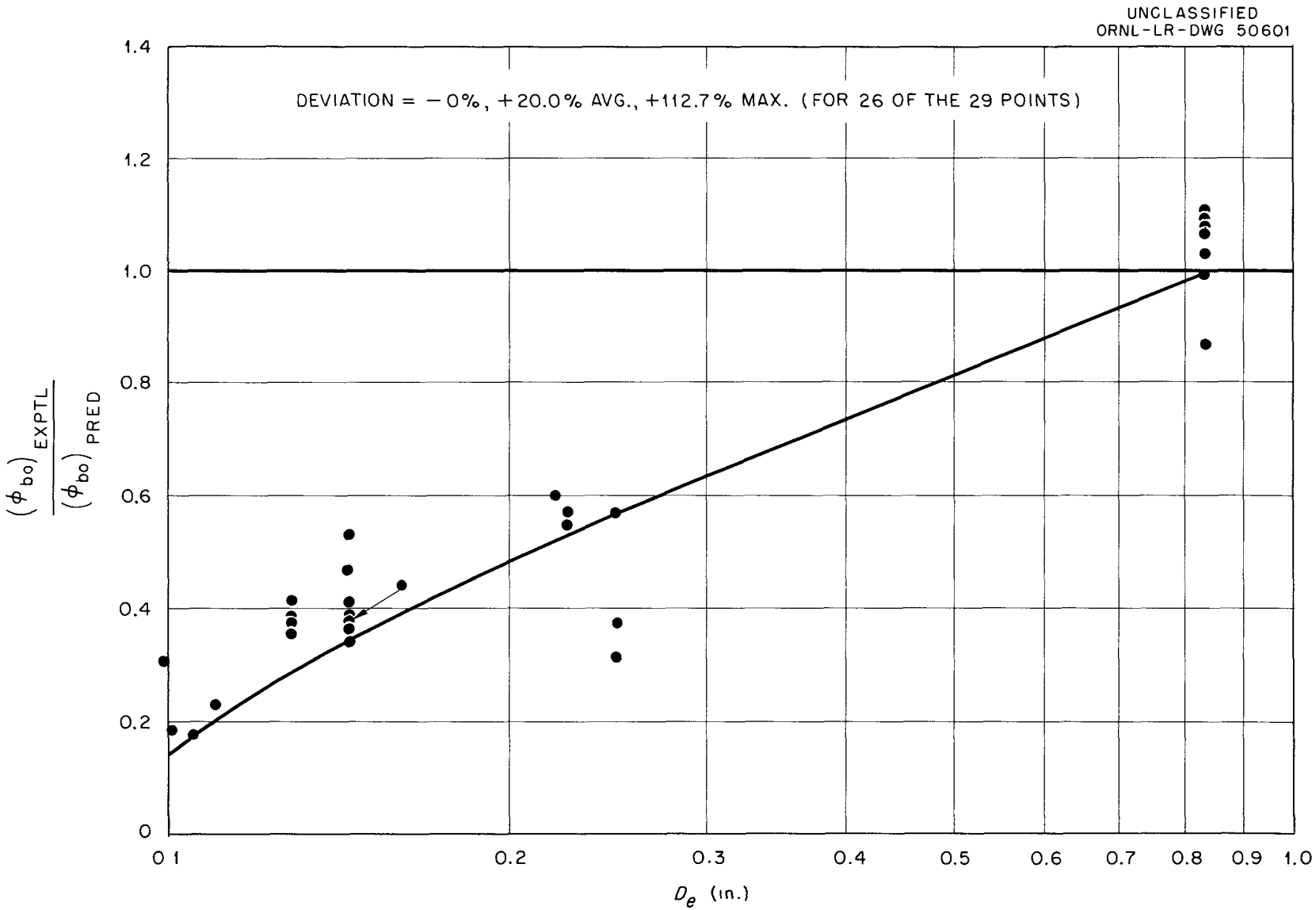

Fig. 9. Variation with Equivalent Diameter of the Ratio of Experimental Natural-Convection Burnout Heat Flux to the Value Predicted by the Correlation of Lee, *et al.*

this study and for the water data of Lee and associates. Tests from Table 1-a for which $A_{TS}/A_D = \infty$ have not been included in Fig. 9, since no method for their correlation presently exists. The burnout heat flux is evidently decreased by smaller equivalent diameters. If the minimum line of Fig. 9 is used to correlate the effect of D_e on burnout heat flux, the method of Lee and associates predicts the experimental values within -0%, +20.0% average, and +112.7% maximum for 26 of the 29 tests.

Heat-Load Method

Most of the attention in heat transfer is usually focused on the heat transferred to the coolant from the heated surface. In the section on modes of burnout, it was pointed out that all the forms of burnout show a critical dependence on the coolant mass velocity. The authors consequently feel that natural-circulation burnout data may also be correlated by considering the heat load, Ψ, defined as the heat removal per unit flow area $\left[\Psi = \phi\ (A_h/A_{TS})\right]$. The burnout heat load has been correlated by the relation:

$$(\Psi_{bo})_{min} = (5.70 \times 10^7)\ \tau\ \pi\ \Lambda\ . \qquad (5)$$

The minimum burnout heat load expected from a 1.00-ft-long channel cooled at atmospheric pressure by natural circulation of saturated water is 5.7×10^7 Btu/hr·ft^2 of flow area.

Figure 10 gives τ, defined as the ratio of burnout heat load obtained with a given subcooling to that obtained with saturated water in the same channel with all other conditions identical, as a function of inlet subcooling. Subcooled inlet water decreases the burnout flux at low pressure because the length of the channel over which bulk boiling occurs (which substantially establishes the density driving pressure for flow) is reduced by the length required to bring the subcooled water to saturation.

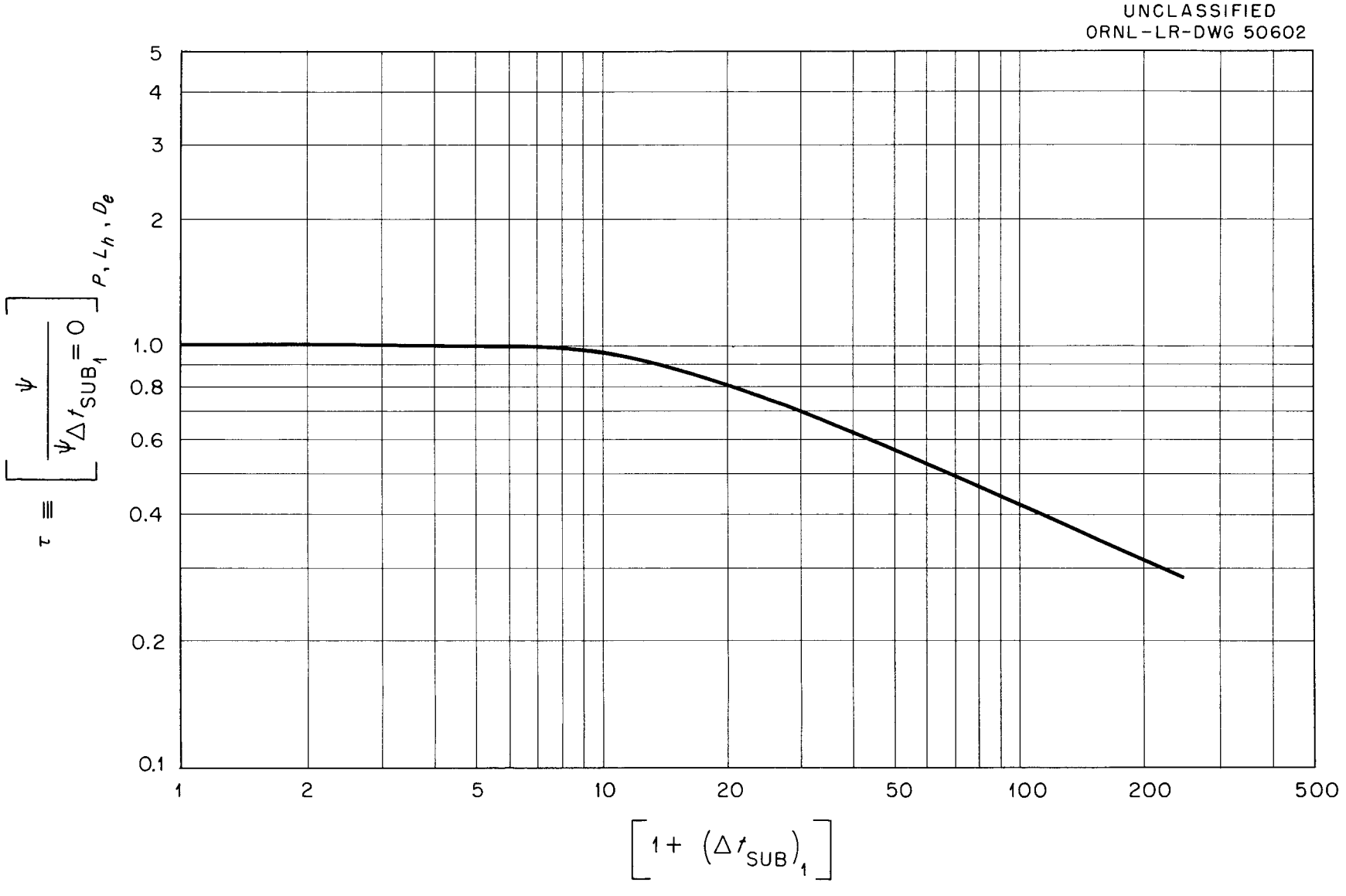

Fig. 10. Effect of Subcooling on Burnout Heat Load.

The effect of pressure on burnout heat load, π (defined as the ratio of the burnout heat load at some pressure to that at atmospheric pressure with all other variables constant), is plotted against pressure in Fig. 11. Increasing pressure increases burnout heat load at low pressure because end, acceleration, and frictional losses are reduced by the greater mixture densities. But increasing pressure lowers burnout heat load at higher pressure by increasing the mixture density so much that the driving pressure is reduced more than are the loss terms.

Figure 12 gives Λ (defined as the ratio of burnout heat load for a channel of a given length to that for a similar channel 1 ft long with all other conditions the same) as a function of length. For short lengths, burnout heat load is increased by lengthening the test section because the driving pressure and the heat-transfer area are increased. However, the frictional pressure drop is also increased, and after this effect becomes controlling, longer channels experience burnout at lower heat loads.

Burnout heat loads have been correlated by the product of the above factors as given in Eq. (5). Experimental burnout heat loads are compared to the predicted values in Fig. 13. The water data of Lee and associates as well as data for unrestricted natural circulation from the present study have been plotted in Fig. 13. Experimental values deviate from the predicted values by -0%, +20.0% average, and +115.1% maximum for 28 of the 30 points used.

The effect of each variable found to be important in natural-circulation burnout has been represented by a single curve. More complete data may reveal that a family of curves, depending on other variables, should be used to represent the effect of each variable. The curves presented have been satisfactorily verified within the range of conditions of the present study. The

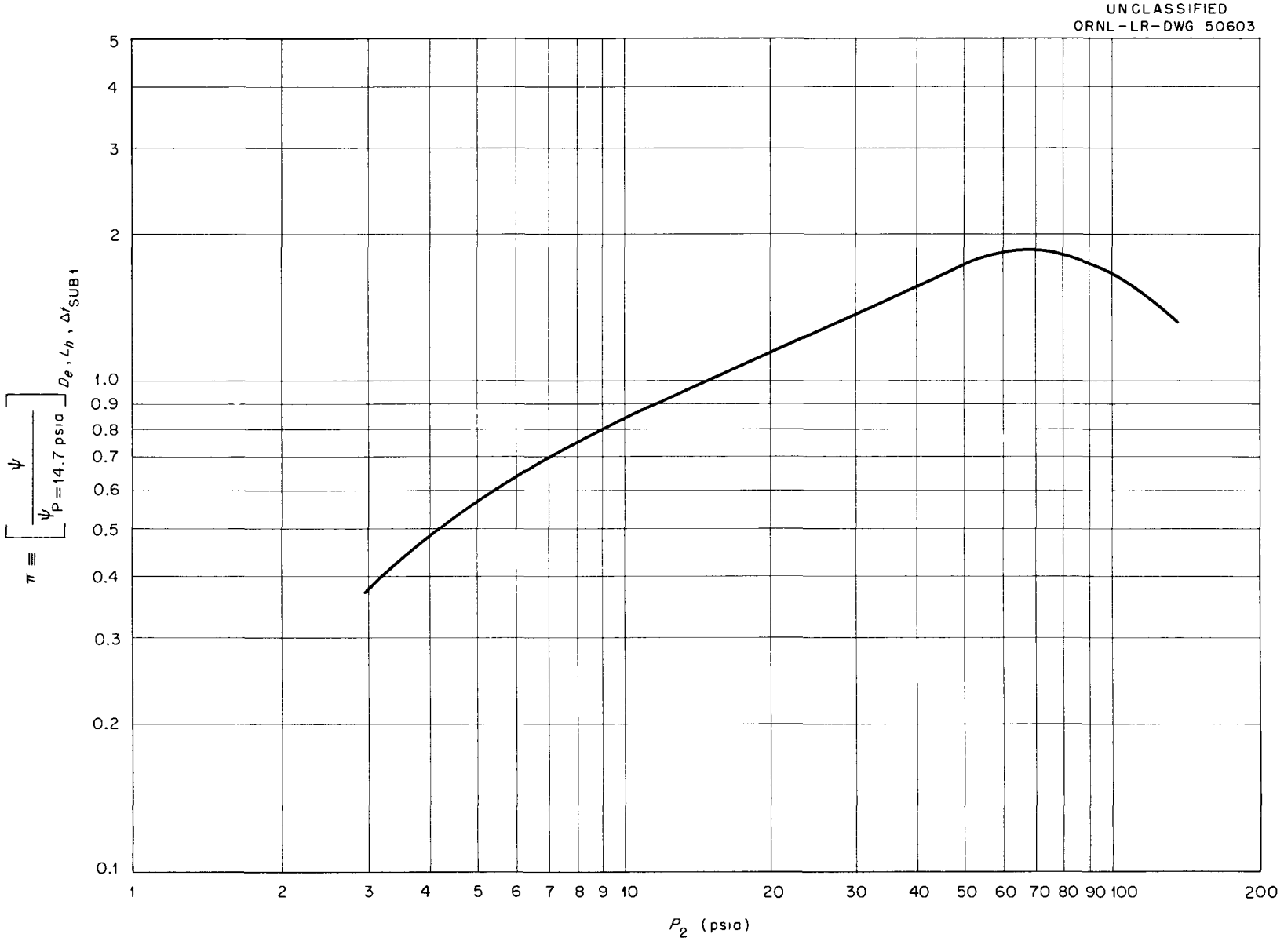

Fig. 11. Effect of Pressure on Burnout Heat Load.

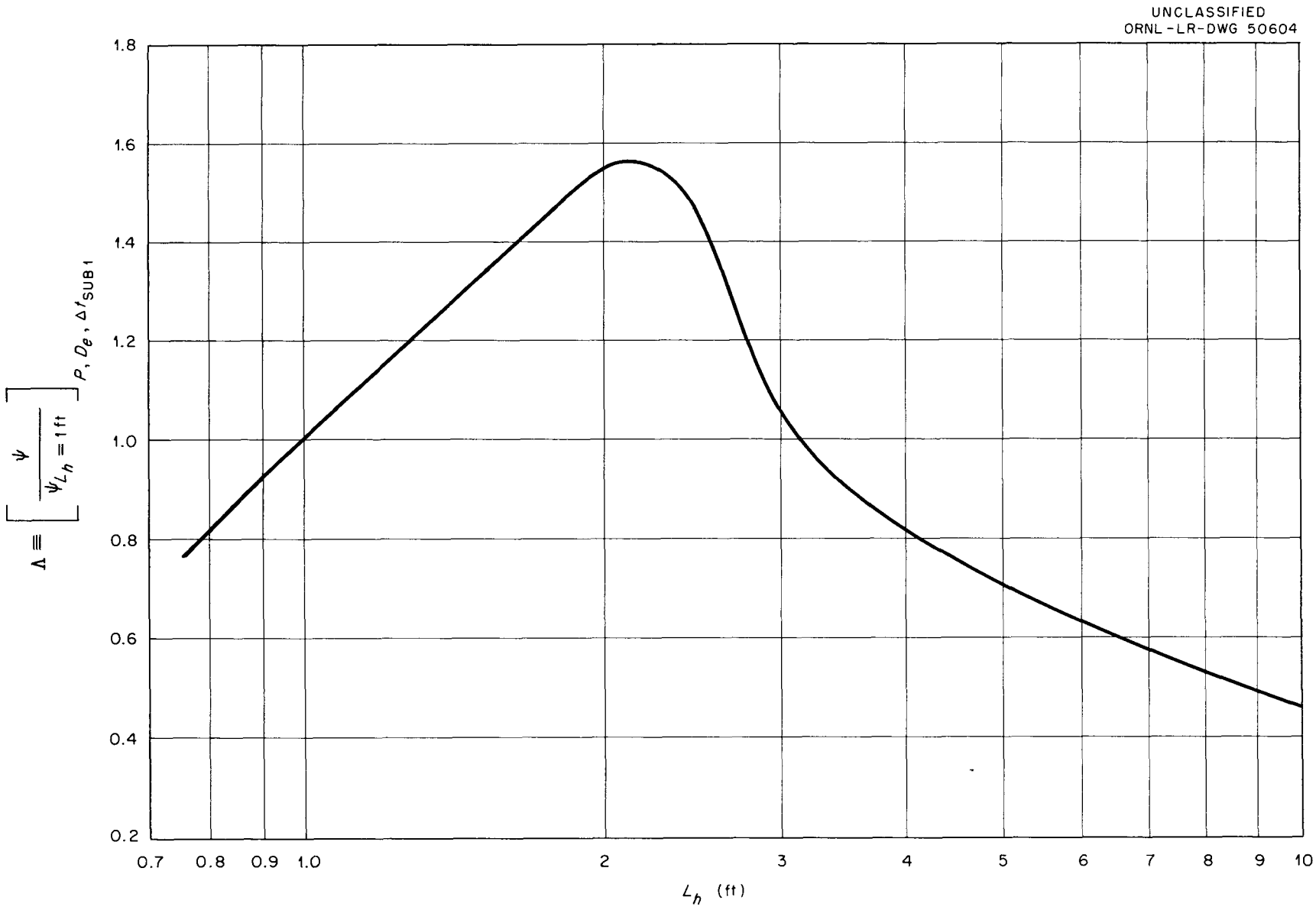

Fig. 12. Effect of Heated Length on Burnout Heat Load.

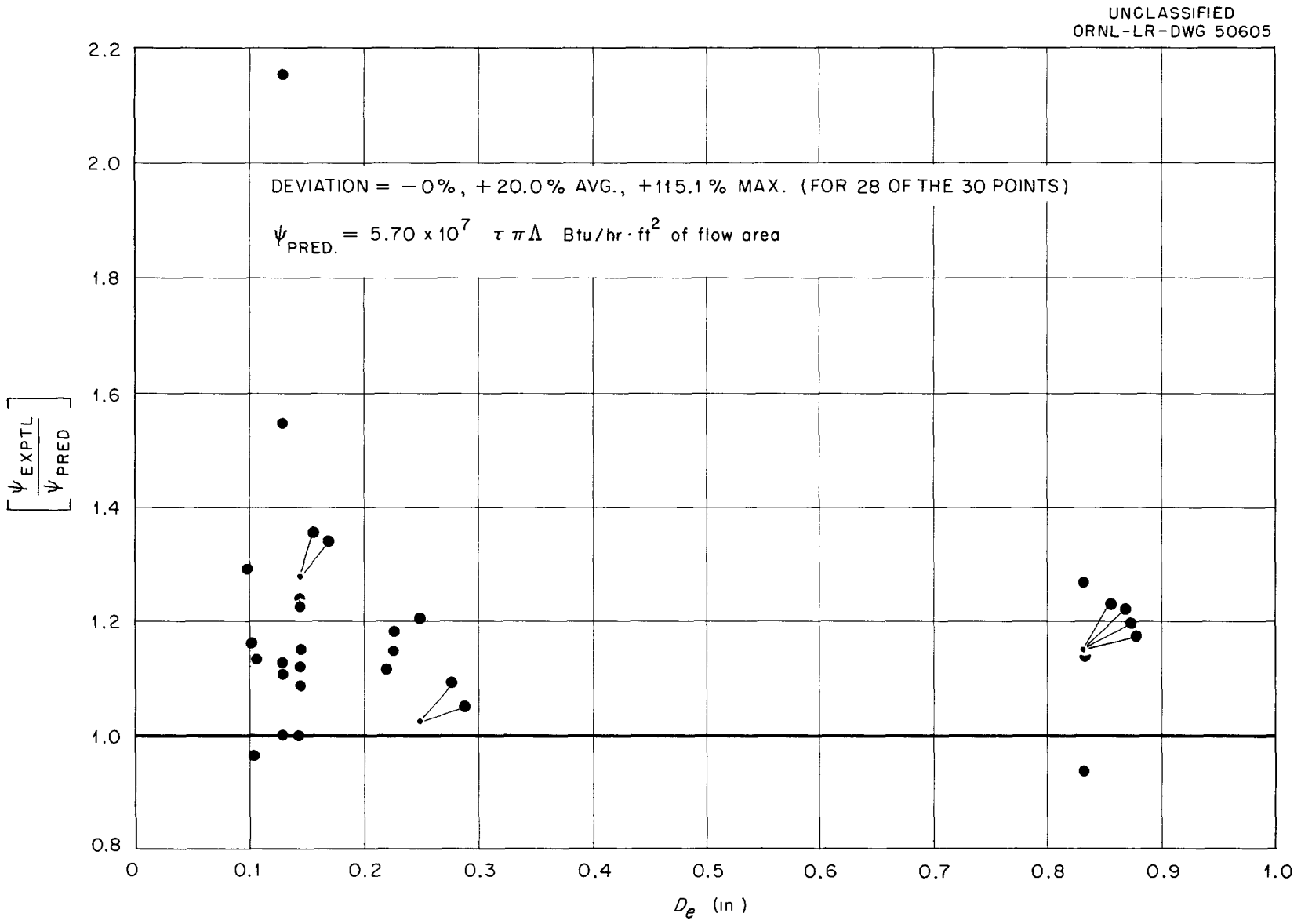

Fig. 13. Experimental Burnout Heat Loads Compared with Values Predicted by Equation (5).

data of Lee and associates have been used to extend the correlation for the effect of pressure on burnout heat load from 27 to 127 psia. However, since subcooling was not varied by Lee and associates, the correlation for the effect of subcooling may not be valid above 27 psia. In particular, Mendler and associates[16] observed that increased subcooling increased burnout heat flux slightly in their tests conducted at 800 to 2000 psia, while Levy and Beckjord[14] found a less positive trend in the same direction at 1000 psia.

The heat-load method is suitable for predicting burnouts that result from impressed heat loads which are too large to be cooled by unrestricted natural circulation. The method is not suitable for prediction of burnouts in channels with hot spots that have much higher heat generation rates than the rest of the channel. For this reason, test 13 has not been included in the comparison of this method with experimental results given in Fig. 13. This method is also not suitable for the prediction of burnouts when the external return path for flow is greatly restricted.

Semitheoretical Prediction Method

Development of Flow Equation.--Figure 14 is a sketch of a typical channel being cooled by natural circulation. The driving pressure causing flow through the channel is:

$$\text{Driving pressure} = (\rho_o - \rho_m)\, L_t\, \frac{g}{g_c} \quad . \tag{6}$$

If the flow area of the channel is small compared to the flow area preceding the entrance, the permanent inlet loss is:

$$\Delta P_i = \frac{1}{2}\, \frac{\rho_o\, V_o^2}{2\, g_c} \quad . \tag{7}$$

In addition to the permanent inlet loss, the inlet pressure is depressed by

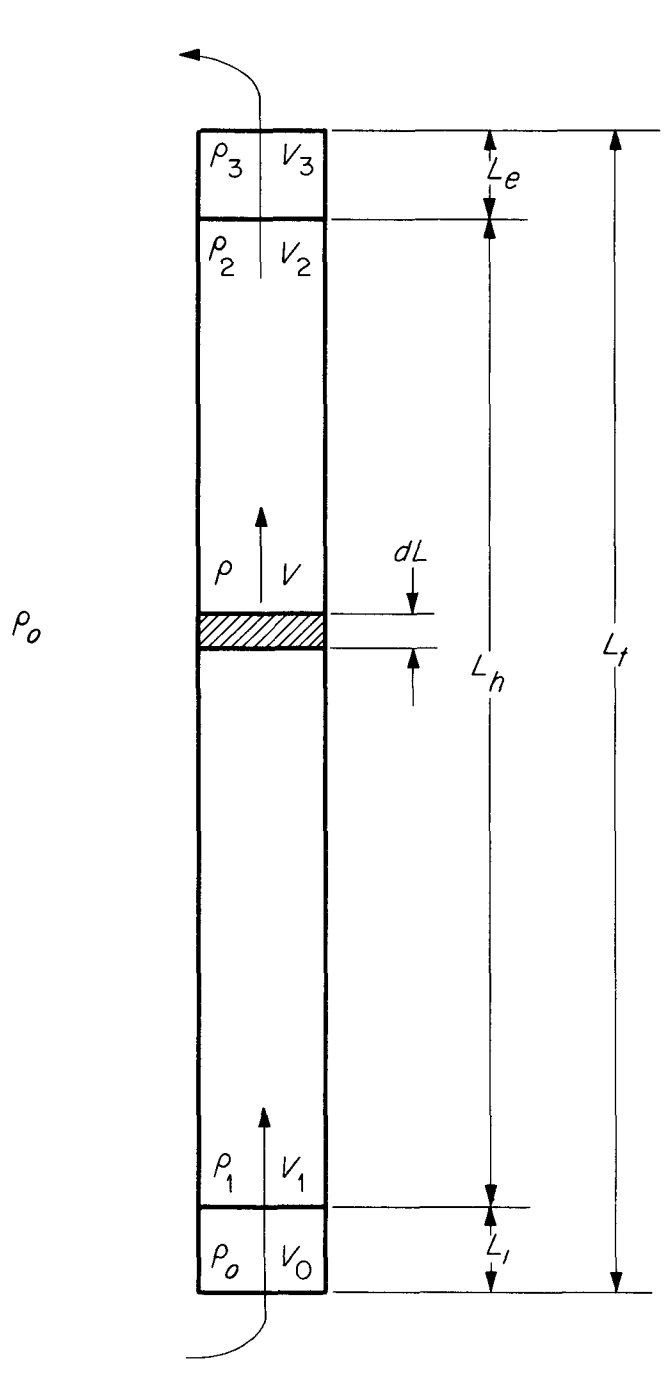

$$\rho_m = \frac{\int_0^{L_t} \rho \, dL}{L_t}$$

Fig. 14. Zones of a Natural-Convection Coolant Channel and Associated Notation.

the transformation of pressure to kinetic energy:

$$\Delta P_B = \frac{\rho_o V_o^2}{2 g_c} \quad . \tag{8}$$

The frictional pressure drop through the channel is:

$$\Delta P_f = \int_0^{L_t} \frac{f \rho V^2}{2 g_c D_e} \, dL \quad . \tag{9}$$

The loss of pressure resulting from the acceleration of the fluid during boiling is:

$$\Delta P_a = \int_{V_1}^{V_2} \frac{\rho V}{g_c} \, dV \quad . \tag{10}$$

If the flow area of the channel is also small compared to the flow area beyond the exit of the channel, none of the kinetic energy is recovered as pressure and all of the above are permanent pressure losses.

The sum of the pressure losses must equal the driving pressure. Combination of Eqs. (6) through (10) in this manner gives the flow equation for natural circulation:

$$(\rho_o - \rho_m) L_t \frac{g}{g_c} = 1.5 \frac{\rho_o V_o^2}{2 g_c} + \int_0^{L_t} \frac{f \rho V^2}{2 g_c D_e} \, dL + \int_{V_1}^{V_2} \frac{\rho V}{g_c} \, dV + \Sigma \Delta P_R \quad , \tag{11}$$

where $\Sigma \Delta P_R$ represents the pressure losses in the flow circuit external to the heated channel. Rathbun, Van Huff, and Weiss[1] in their report on natural-circulation heat transfer and burnout, and Fair[17] in his article on heat transfer in thermosiphon reboilers, among others, have developed flow equations similar to Eq. (11).

In many cases near burnout, the resistance to flow through the return leg is small compared to that through the channel itself and may be neglected. The acceleration term may be integrated by substitution of $\rho V = G$ = constant. The friction term in Eq. (11) may be approximately integrated by using the mean fluid density inside the channel if the friction factor is evaluated from a Reynolds number based on the liquid viscosity at the boiling point.[18] The homogeneous model will be used throughout this section, although an appropriate model accounting for slip can be used with Eq. (11). Justification for use of the homogeneous model will be given in a later section.

Integration of Eq. (11) gives:

$$(\rho_o - \rho_m) L_t \frac{g}{g_c} = 1.5 \frac{\rho_o V_o^2}{2 g_c} + \frac{f \rho_m V_m^2 L_t}{2 g_c D_e} + \frac{G}{g_c} (V_2 - V_1) . \quad (12)$$

Equation (12) may be more easily used to calculate the flow at burnout if it is written in terms of the mass velocity:

$$(\rho_o - \rho_m) L_t \frac{g}{g_c} = 1.5 \frac{G^2}{2 g_c \rho_o} + \frac{f G^2 L_t}{2 g_c D_e \rho_m} + \frac{G^2}{2 g_c} \left(\frac{2}{\rho_2} - \frac{2}{\rho_1} \right) . \quad (13)$$

Equation (13) may be rearranged to give:

$$G^2 = \frac{2 g (\rho_o - \rho_m) L_t}{\frac{f L_t}{D_e \rho_m} + \frac{2}{\rho_2} - \frac{0.5}{\rho_o}} . \quad (14)$$

Resistances to flow in the return path may be considered by adding terms for these resistances to the denominator of the right side of Eq. (14). In the swirl-flow tests, g in Eq. (14) was taken as normal earth gravity, since the centrifugal acceleration associated with the rotating coolant acts in a different plane than the vertical convective driving force which

establishes coolant flow.

Burnout Equations.--Any reliable burnout correlation applicable to bulk boiling may be used. The nature of the correlation should be such that the burnout may be easily calculated from a knowledge of the channel geometry, the fluid conditions at the burnout location, and the mass flow rate. The authors prefer Lowdermilk's correlations[19] for straight-flow burnout:

$$\phi_{bo} = \frac{(2.85 \times 10^5)\, G^{0.85}}{D_e^{0.2} \left(\frac{L_h}{D_e} \right)^{0.85}} \tag{15}$$

for $\dfrac{G}{\left(\frac{L_h}{D_e} \right)^2} < 0.042$, or

$$\phi_{bo} = \frac{(8.40 \times 10^4)\, G^{0.5}}{D_e^{0.2} \left(\frac{L_h}{D_e} \right)^{0.15}} \tag{16}$$

for $\dfrac{G}{\left(\frac{L_h}{D_e} \right)^2} > 0.042$, and the equation[20]:

$$\phi_{bo,avg} = \frac{(1.56 \times 10^5)\, G^{0.645} \left(D_i \right)_{in.}^{0.24} \left(1 + \frac{\pi^2}{4\, y^2} \right)^{0.323}}{\left(L_h \right)_{in.}^{0.44}} \tag{17}$$

for burnout in tubes with full-length internal twisted tapes. The conditions of this study were such that Eq. (15) was always used for straight-flow burnouts. Lowdermilk's correlations[19] were derived from burnout data for water at pressures from atmospheric to 100 psia. A 15% increase in burnout heat flux was noted by Lowdermilk when pressure was increased from atmospheric to

100 psia. No pressure effect was noted in the data used to develop Eq. (17).

Calculation Procedure.--The following method of performing the necessarily iterative calculation is recommended:

1. Assume an exit quality; then

$$\Delta H_t = \Delta H_{sub} + x_e (\Delta H_{fg}) . \tag{18}$$

2. Calculate the driving pressure arising from the difference in densities inside and outside the heated channel. Figure 15 indicates how this can easily be done. The liquid will remain at the inlet density until it reaches the heated portion of the channel. The liquid density will then decrease fairly uniformly to its saturation value as the coolant progresses along the heated length. After boiling begins, the fluid density will decrease sharply, approaching its final value. The fluid density will remain at its final value from the end of the heated length to the channel exit. The density curve during vaporization may be obtained by plotting the density at various vapor qualities against the length at which each quality would be attained, where this length is:

$$L_x = L_i + \left(\frac{\Delta H_{sub} + x \Delta H_{fg}}{\Delta H_t} \right) L_h \tag{19}$$

if the heat flux is fairly uniform along the channel. If the axial heat-flux distribution is highly nonuniform, this fact must be taken into account in calculating the position at which a given vapor quality will occur. The density at a given vapor quality may be calculated from a homogeneous model:

$$\rho_x = \frac{1}{x v_v + (1 - x) v_\ell} \tag{20}$$

The pressure drop through the channel is usually so small compared to the

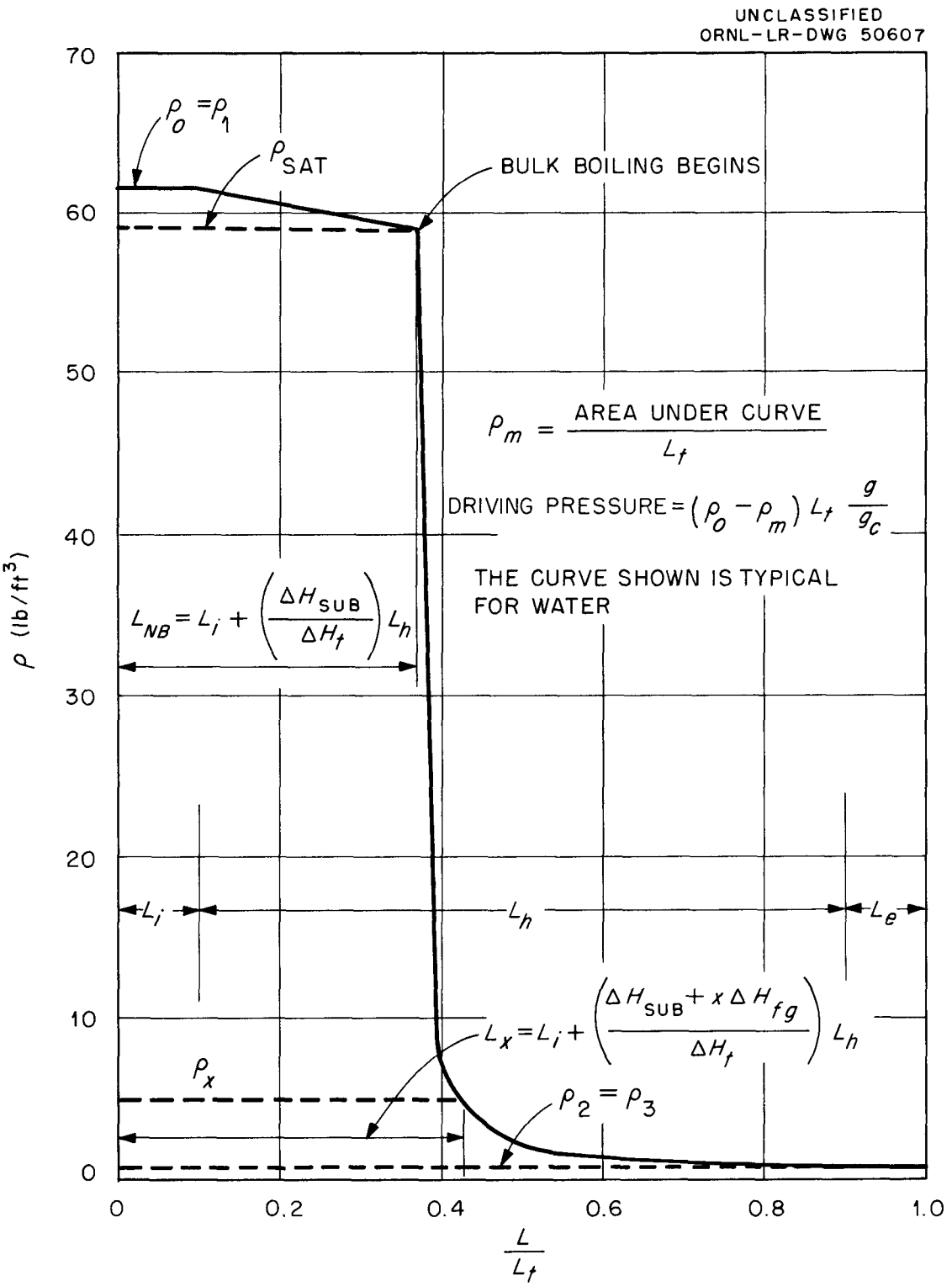

Fig. 15. Calculation of Driving Pressure Based on a Homogeneous-Flow Model.

system pressure that the pressure at the channel flow exit may be used in determining the vapor density throughout the channel. The mean fluid density in the channel is the area under the curve of density versus channel length, divided by the channel length. Equation (6) can then be used to calculate the driving pressure.

3. Calculate the resistance to flow by substituting the mean density and the entrance density into the denominator of Eq. (14). The exit density, ρ_2, may be calculated from the assumed exit vapor quality by using Eq. (20). The friction factor should be evaluated from a Reynolds number calculated using the liquid viscosity at the saturation temperature.

4. Solve Eq. (14) for the mass velocity. Some trial and error may be required since the friction factor depends on the mass velocity. However, the frictional resistance is usually only a small part of the total resistance, and the trial-and-error calculation converges quickly to a solution.

5. Solve for the burnout heat flux at the assumed exit vapor quality by substituting the calculated mass velocity into Eq. (15), (16), or (17).

6. Calculate the heat transferred at this heat flux:

$$q = \phi_{bo} A_h . \tag{21}$$

This is the maximum heat-transfer rate at the calculated mass velocity.

7. Calculate the heat needed to give the assumed exit vapor quality:

$$q' = 3600 \Delta H_t G A_{TS} . \tag{22}$$

The ratio of q to q' is the same as the largest ratio of maximum to average heat flux which could be sustained at an average heat flux of $\phi_{avg} = (q'/A_h)$.

8. Repeat the above procedure and plot the results as q/q' versus ϕ_{bo}. Usually three points are enough to establish a satisfactory plot. Figure 16 is typical of such a plot. The burnout heat flux is the heat flux at which the line of q/q' versus ϕ_{bo} crosses the ratio of maximum to average heat flux characteristic of the particular channel. The burnout vapor quality and the mass velocity at burnout may be determined in the same manner.

Burnouts Not Caused by Film Boiling.--As explained in the section on modes of burnout, a heated channel may burn out in two ways before film boiling begins.

If the channel burns out because the coolant can remove only a certain amount of heat, the plot of the heat transferred, q', against exit vapor quality will have a maximum while the value of q/q' is greater than ϕ_{max}/ϕ_{avg}. The heat transferred at burnout will be the maximum value of q' attained. The calculated burnout heat flux will be that value of heat transferred divided by the heated area and multiplied by the ratio of ϕ_{max}/ϕ_{avg} characteristic of the channel:

$$\left(\phi_{bo} \right)_{max} = \frac{q'}{A_h} \left(\frac{\phi_{max}}{\phi_{avg}} \right). \qquad (23)$$

Also, the exit vapor quality may reach 100% while q/q' is greater than ϕ_{max}/ϕ_{avg}. The heat transferred at burnout is the value of q' when the exit quality reaches 100%. The burnout heat flux for this case is calculated by substituting the value of q' at 100% exit quality into Eq. (23). The burnout heat flux at 100% exit quality can also be obtained by dividing the value of ϕ_{bo} (calculated from a film-boiling burnout correlation) at which the exit quality reaches 100% by the ratio of q/q' at 100% exit quality and multiplying by ϕ_{max}/ϕ_{avg}:

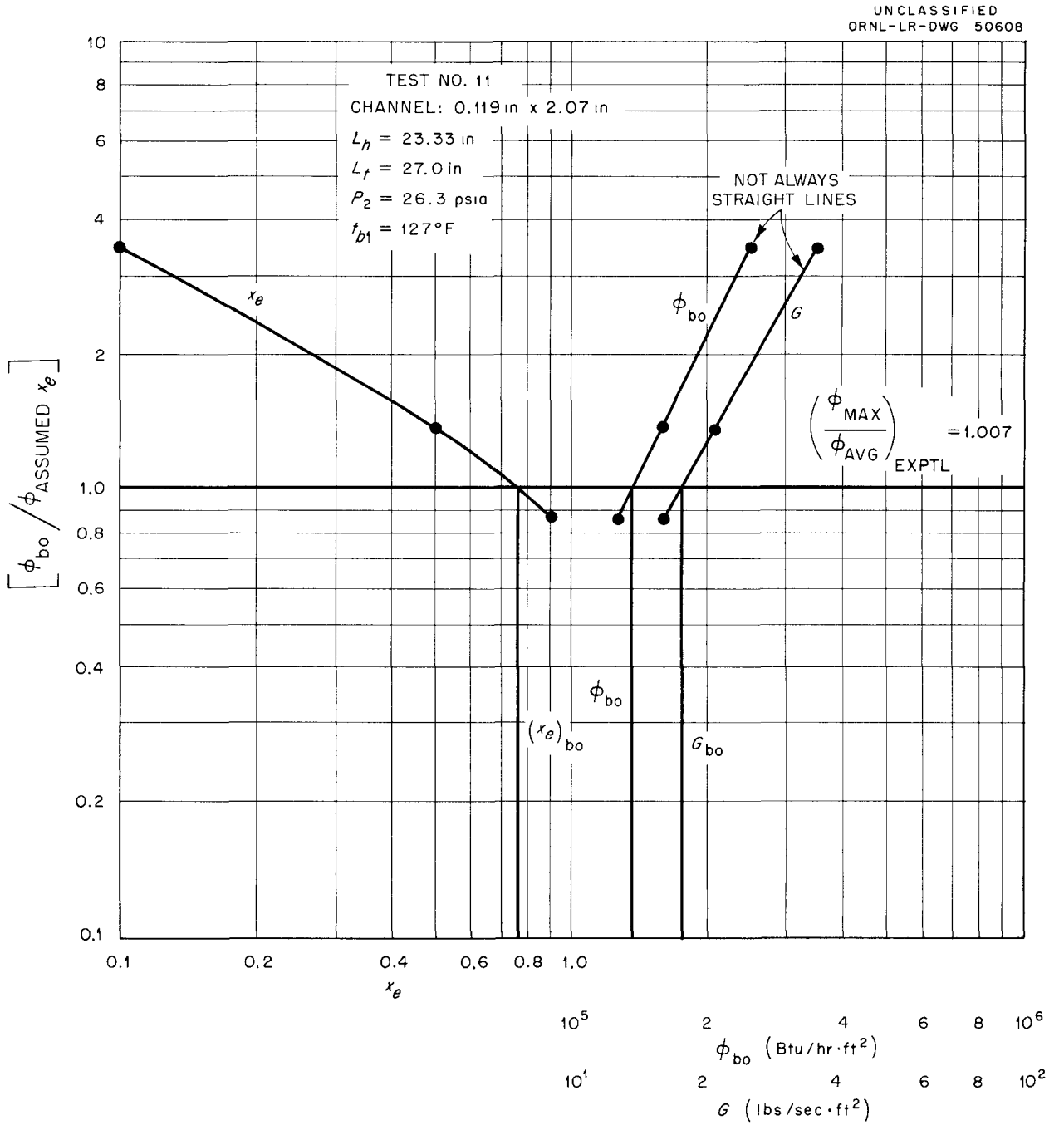

Fig 16 Summary of Sample Burnout Calculation.

$$\left(\phi_{bo}\right)_{max} = \left(\phi_{bo}\right)_{x_e=100\%} \left(\frac{q'}{q}\right)_{x_e=100\%} \left(\frac{\phi_{max}}{\phi_{avg}}\right) . \qquad (24)$$

Comparison with Experimental Results.--Figure 17 is a comparison of burnout heat fluxes calculated by the preceding method to the experimental values obtained in the present study. The agreement is good (14.7% and 38.3% average and maximum errors for all the data), but the predicted values tend to be high at high inlet subcooling. As minimum design values, the authors recommend the use of 0.7 $(\phi_{bo})_{pred}$ for $(\Delta t_{sub})_1 \geq 130°F$, 0.8 $(\phi_{bo})_{pred}$ for $80°F < (\Delta t_{sub})_1 < 130°F$, and 0.9 $(\phi_{bo})_{pred}$ for $(\Delta t_{sub})_1 < 80°F$.

The authors have not tested the prediction method for liquids other than water, pressures greater than 27 psia, or flow channels with equivalent diameters greater than 0.25 in.

Comparison of Results Obtained Using Slip with Experimental Data

A homogeneous model has been used to evaluate the densities and acceleration and frictional losses in the previous method. Although the burnout values predicted by the previous method are in reasonable agreement with the experimental burnouts, the inhomogeneity observed by those who have investigated two-phase flow has led the authors to also calculate natural-circulation burnout fluxes using a model which considers slip between the two phases.

The authors have chosen the Martinelli correlations for use in the slip calculations because of their wide application. The average two-phase friction multiplier for a channel with uniform heat input was taken from the report of Lottes, Petrick, and Marchaterre.[21] The original Lockhart and Martinelli correlations[5] have been used for density calculations and for the two-phase friction multiplier for the isothermal section just preceding the

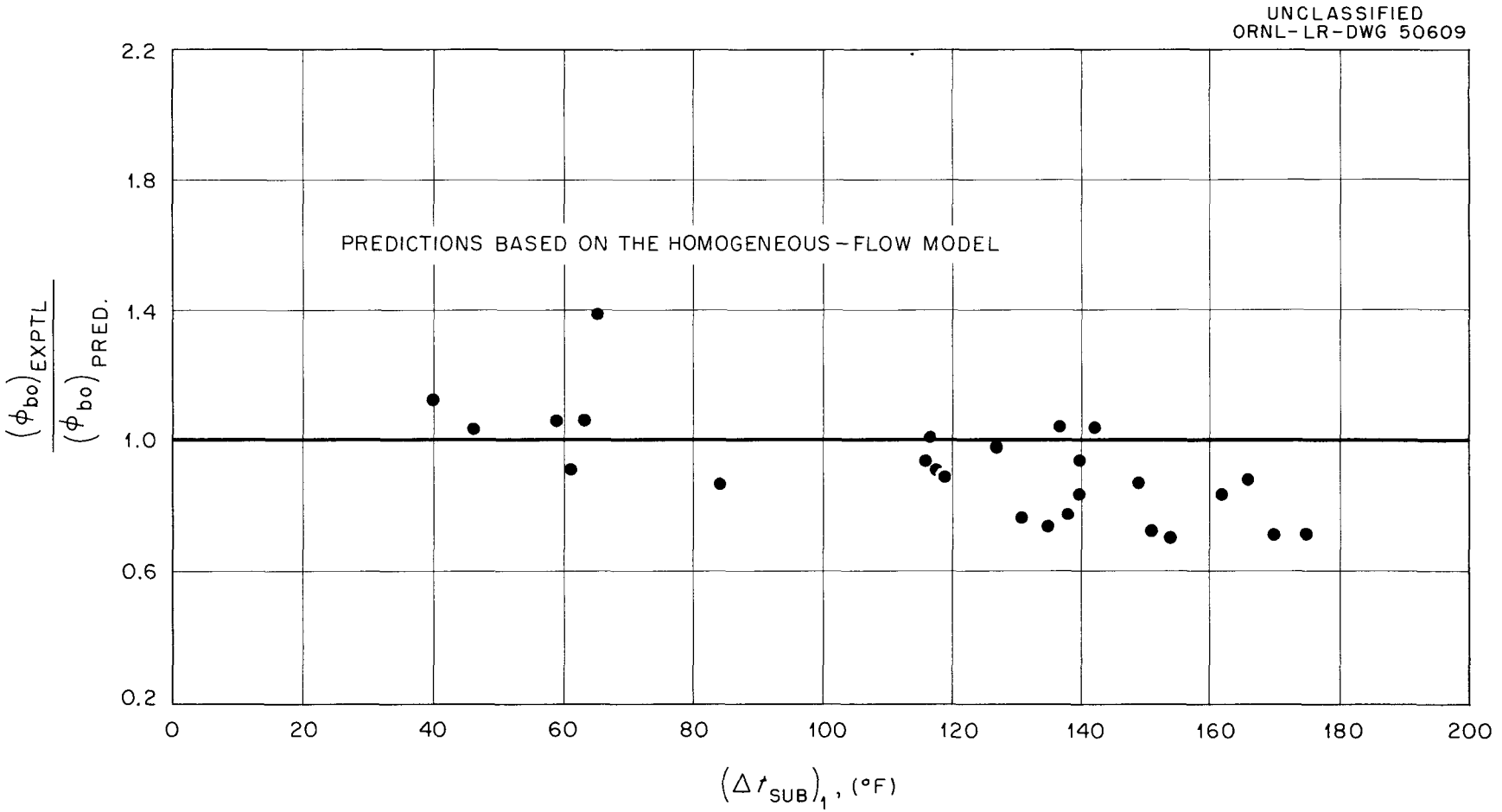

Fig. 17. Comparison of Experimental and Predicted Values of Burnout Heat Flux.

flow exit of the channel. The acceleration loss in boiling two-phase flow was evaluated with the Martinelli-Nelson correlation.[6]

Equation (14), when modified to account for slip, becomes:

$$G^2 = \frac{2\, g\, (\rho_o - \rho_m)\, L_t}{\frac{\bar{R}\, f\, L_h}{D_e\, \rho_{sat}} + 2\, r + \frac{1.5}{\rho_l} + \frac{\phi_l^2\, f\, L_e}{D_e\, \rho_{sat}} + \frac{f\, L_i}{D_e\, \rho_l}} \cdot \qquad (25)$$

The mean density is evaluated by the same method as before, but with the density at each quality calculated from the Lockhart-Martinelli correlation.[5] The method for predicting burnout is the same as that for a homogeneous model except for the modifications in calculating the mass velocity.

The ratio of the experimental burnout heat flux to that calculated accounting for slip with Martinelli-type correlations is plotted against equivalent diameter in Fig. 18. The calculations using slip generally result in higher calculated exit vapor qualities and smaller predicted heat fluxes at burnout.

The burnout heat fluxes predicted using slip do not agree with the experimental values nearly as well as do those predicted using the homogeneous model. The equivalent diameter appears to have a marked effect on the degree of slip. The predicted burnouts come fairly close to the experimental values for the largest equivalent diameters used (0.22 to 0.25 in.), but are grossly in error for the smaller equivalent diameters tested. This effect leads the authors to conclude that slip is inhibited by small flow channels. The above conclusion is in agreement with the previously cited data of Govier and Short[7] and of Bailey et al.[12]

Swirl flow tests 22 through 29, however, are exceptions to such a trend, since burnout heat fluxes calculated from a slip model agree very well with

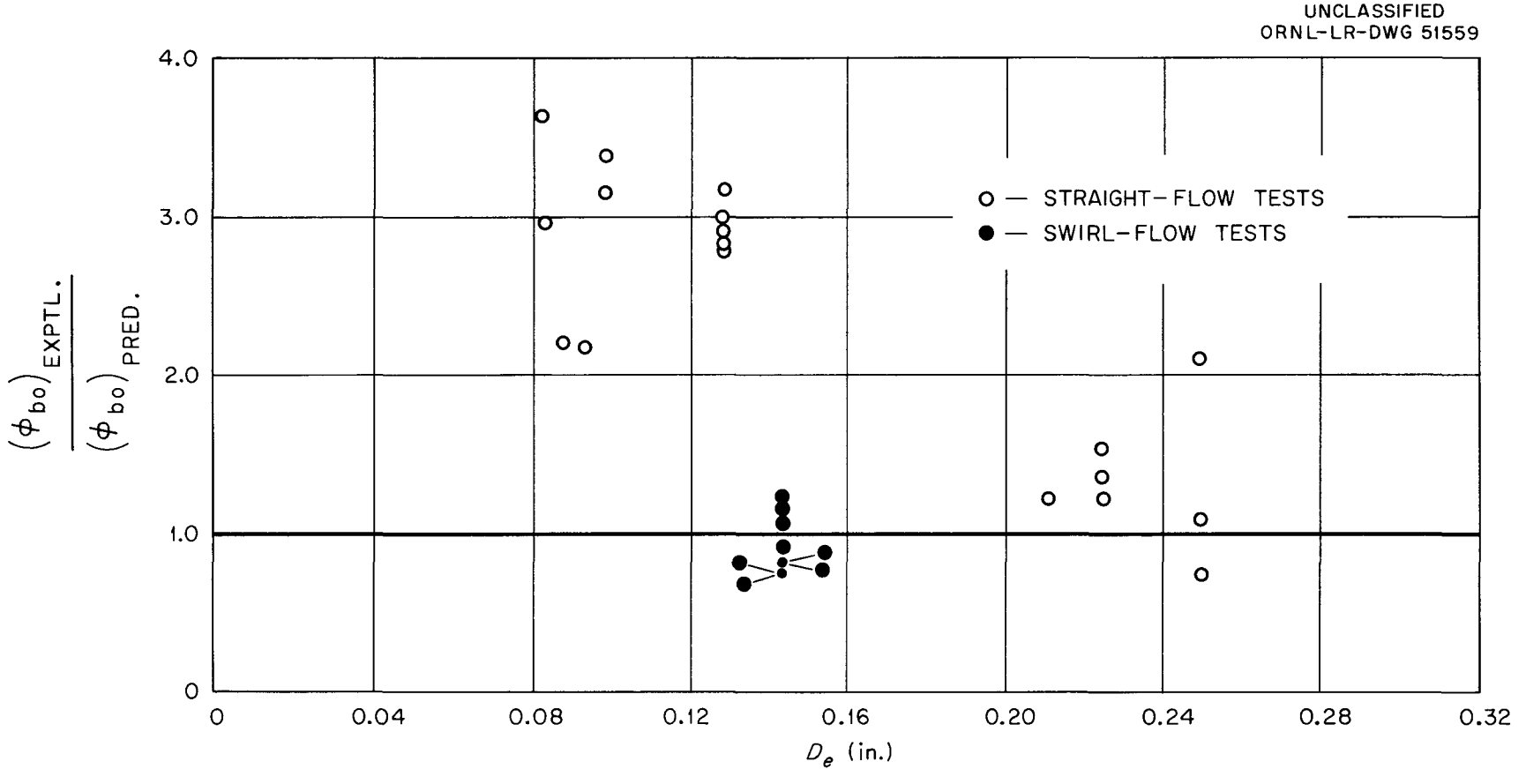

Fig.18. Comparison of Experimental and Predicted Values of Burnout Heat Flux – Predictions Based on Martinelli–Nelson and Lockhart–Martinelli Correlations.

the experimental values, even though D_e was only 0.144 in. The centrifugal acceleration of the liquid toward the wall in this case doubtless favored an annular flow pattern and a greater opportunity for slip to occur.

Since the burnout heat fluxes calculated using slip do not agree well with experimental data, while those calculated using a homogeneous model do, the authors recommend the use of the homogeneous model with the method described in this report for the prediction of natural-circulation burnout heat fluxes for low-pressure water in channels with equivalent diameters less than 0.25 in.

ACKNOWLEDGMENT

The authors wish to express their appreciation to J. Lones and D. H. Wallace for their able and enthusiastic assistance as project technicians, and to Dolores Eden for her conscientious typing of the manuscript.

NOTATION

(Listed units are used except where otherwise noted)

A	area, ft^2
C_p	heat capacity at constant pressure, $Btu/lb_m \cdot °F$
D	diameter, ft
f	friction factor, dimensionless
G	mass velocity, $lb_m/sec \cdot ft^2$
g	gravitational acceleration, ft/sec^2
g_c	conversion constant, $32.17\ ft \cdot lb_m/lb_f \cdot sec^2$
ΔH	change of enthalpy, Btu/lb
k	thermal conductivity, $Btu/hr \cdot ft^2 \cdot °F/ft$
L	length, ft
M	molecular weight, lb/lb·mole
P	static pressure, psia
ΔP	pressure drop, psf
Pr	Prandtl number, $C_p\mu/k$, dimensionless
q	heat transferred at trial burnout heat flux, Btu/hr
q'	heat removed by coolant, Btu/hr
$\overline{R}$	average friction-factor multiplier, dimensionless
r	Martinelli-Nelson two-phase acceleration loss factor, ft^3/lb_m
t	temperature, °F
Δt	temperature difference, °F
Δt_{sub}	degree of subcooling, $(t_{sat} - t_b)$, °F
V	velocity, ft/sec
v	specific volume, ft^3/lb_m

X dimensional correlation factor of Lee and associates [see Eq. (3)]

x wall thickness, ft; also vapor quality, i.e., flowing weight-fraction vapor, dimensionless

Y dimensional correlation factor of Lee and associates [see Eq. (4)]

y tape twist ratio, inside diameters/180-deg twist

Λ ratio of burnout heat load for a channel of a given length to that for a similar channel 1 ft long with all other conditions the same, dimensionless

μ dynamic viscosity, $lb_m/ft \cdot sec$

π ratio of the burnout heat load at some pressure to that at atmospheric pressure, dimensionless

ρ density, lb_m/ft^3

σ surface tension, lb_f/ft

τ ratio of burnout heat load obtained with a given subcooling to that obtained with saturated water, dimensionless

ϕ heat flux, $Btu/hr \cdot ft^2$ of heated surface

ϕ^2 Lockhart-Martinelli two-phase friction-factor multiplier

ψ heat load, $Btu/hr \cdot ft^2$ of test-section flow area

Subscripts

a resulting from fluid acceleration

avg average value for test section

B resulting from kinetic energy increase

b bulk

bo at burnout

D of downcomer flow cross section

e equivalent; also exit

exptl experimental value

f resulting from wall friction; also across film

fg	from liquid to vapor
h	heated
i	inlet; also inside
ℓ	of liquid
m	mean value in test section
max	maximum value for test section
NB	nonboiling
o	mean value outside test section
pred	predicted value
R	in flow circuit external to the test section
sat	at saturation
sub	subcooled
t	total
TS	of test-section flow cross section
v	of vapor
w	across the heated wall
x	at a given quality
0	at test-section entrance
1	at beginning of heated length
2	at end of heated length
3	at test-section exit

REFERENCES

1. A. S. Rathbun, N. E. Van Huff, and A. Weiss, Natural Circulation of Water at 1200 Psia Under Heated, Local Boiling and Bulk Boiling Conditions: Test Data and Analysis, WAPD-AD-TH-470 (December 1958).

2. K. Goldmann, H. Firstenberg, and C. Lombardi, Burnout in Turbulent Flow – A Droplet Diffusion Model, ASME Preprint No. 60-HT-34, Fourth National Heat Transfer Conference, Buffalo, N. Y. (Aug. 14 – 17, 1960).

3. H. S. Isbin, Two-Phase Heat Transfer, Two-Phase Burnout, AECU-4305 (1959).

4. G. W. Govier, B. A. Radford, and J. C. Dunn, "The Upwards Vertical Flow of Air-Water Mixtures: I. Effect of Air and Water Rates on Flow Pattern, Holdup and Pressure Drop," J. Can. Chem. Eng. 35, 58 (1957).

5. R. W. Lockhart and R. C. Martinelli, "Proposed Correlation of Data for Isothermal Two-Phase, Two-Component Flow in Pipes," Chem. Eng. Prog. 45, 39 (1949).

6. R. C. Martinelli and D. B. Nelson, "Prediction of Pressure Drop During Forced Circulation of Boiling Water," Trans. ASME 70, 695 (1948).

7. G. W. Govier and W. L. Short, "The Upward Vertical Flow of Air-Water Mixtures: II. Effect of Tubing Diameter on Flow Pattern, Holdup and Pressure Drop," J. Can. Chem. Eng. 36, 195 (1958).

8. R. A. S. Brown, G. A. Sullivan, and G. W. Govier, "The Upward Vertical Flow of Air-Water Mixtures: III. Effect of Gas Phase Density on Flow Pattern, Holdup and Pressure Drop," J. Can. Chem. Eng. 37, 62 (1960).

9. G. E. Alves, "Co-Current Liquid-Gas Flow in a Pipeline Contactor," Chem. Eng. Prog. 50, 449 (1953).

10. O. Baker, "Simultaneous Flow of Oil and Gas," Oil and Gas Journal 53, 185 (1954).

11. H. S. Isbin et al., "Two-Phase Steam-Water Pressure Drops," CEP Symposium Series, Nuclear Engineering 55, No. 23, Part VI, p 75-84 (1959).

12. R. V. Bailey et al., Transport of Gases Through Liquid-Gas Mixtures, ORNL CF-55-12-118 (Dec. 21, 1955).

13. E. R. Quandt, Analysis and Measurement of Flow Oscillations, AIChE Preprint No. 27, Fourth National Heat Transfer Conference, Buffalo, N. Y. (Aug. 14 – 17, 1960).

14. S. Levy and E. S. Beckjord, Hydraulic Instability in a Natural Circulation Loop with Net Steam Generation at 1000 Psia, ASME Preprint No. 60-HT-27, Fourth National Heat Transfer Conference, Buffalo, N. Y. (Aug. 14 – 17, 1960).

15. D. C. Lee, J. W. Dorsey, G. Z. Moore, and F. D. Mayfield, "Design Data for Thermosiphon Reboilers," Chem. Eng. Prog. 52, No. 4, 160 (1956).

16. O. J. Mendler, A. S. Rathbun, N. E. Van Huff, and A. Weiss, Natural Circulation Tests with Water at 800 to 2000 Psia Under Nonboiling, Local Boiling and Bulk Boiling Conditions, ASME Preprint No. 60-HT-36, Fourth National Heat Transfer Conference, Buffalo, N. Y. (Aug. 14 - 17, 1960).

17. J. R. Fair, "What You Need to Design Thermosiphon Reboilers," Petroleum Refiner 39, 105 (1960).

18. D. Q. Kern, Process Heat Transfer, p 463, McGraw-Hill, New York, 1950.

19. W. H. Lowdermilk, C. D. Lanzo, and B. L. Siegel, Investigation of Boiling Burnout and Flow Stability for Water Flowing in Tubes, NACA-TN-4382 (September 1958).

20. W. R. Gambill, R. D. Bundy, and R. W. Wansbrough, Heat Transfer, Burnout, and Pressure Drop for Water in Swirl Flow Through Tubes with Internal Twisted Tapes, ORNL-2911 (Mar. 28, 1960).

21. P. A. Lottes, M. Petrick, and J. F. Marchaterre, Lecture Notes on Heat Extraction from Boiling Water Power Reactors, ANL-6063, p 31 (October 1959).

ORNL-3026
UC-80 - Reactors-General
TID-4500 (15th ed.)

INTERNAL DISTRIBUTION

1. L. G. Alexander
2. C. F. Allen (K-25)
3. F. T. Binford
4. E. P. Blizard
5. R. B. Briggs
6-16. R. D. Bundy
17. C. A. Burchsted
18. C. E. Center
19. T. G. Chapman
20. R. A. Charpie
21. R. D. Cheverton
22. H. C. Claiborne
23. R. S. Cockreham
24. T. E. Cole
25. C. W. Collins
26. J. W. Cooke
27. F. L. Culler
28. L. B. Emlet
29. E. P. Epler
30. W. K. Ergen
31. A. P. Fraas
32. W. R. Gall
33-63. W. R. Gambill
64. W. F. Gauster
65. J. P. Gill
66. J. C. Griess
67. L. A. Haack
68. D. C. Hamilton
69. R. J. Hefner
70. R. L. Higgins (K-25)
71. N. Hilvety
72-75. H. W. Hoffman
76. L. B. Holland
77. W. H. Jordan
78. P. R. Kasten
79. C. P. Keim
80. M. T. Kelley
81. J. J. Keyes, Jr.
82. G. J. Kidd, Jr.
83. W. Kofink
84. A. I. Krakoviak
85. J. A. Lane
86. C. G. Lawson
87. J. S. Lewin
88. R. S. Livingston
89. J. Lones
90. M. I. Lundin
91. J. N. Luton
92. F. E. Lynch
93. R. N. Lyon
94. H. G. MacPherson
95. E. R. Mann
96. T. H. Mauney
97. H. A. McLain
98. J. R. McWherter
99. J. W. Michel
100. C. S. Morgan
101. K. Z. Morgan
102. J. P. Murray (Y-12)
103. M. L. Nelson
104. R. H. Nimmo
105. L. C. Oakes
106. D. Phillips
107. C. A. Preskitt
108. P. M. Reyling
109. M. W. Rosenthal
110. H. C. Savage
111. H. E. Seagren
112. E. D. Shipley
113. M. J. Skinner
114. A. H. Snell
115. I. Spiewak
116. W. J. Stelzman
117. R. S. Stone
118. J. A. Swartout
119. E. H. Taylor
120. M. Tobias
121. J. N. Turpin (Y-12)
122. W. E. Unger
123. D. H. Wallace
124. J. L. Wantland
125. A. M. Weinberg
126. J. F. Wett, Jr.
127. M. E. Whatley
128. C. E. Winters
129. M. M. Yarosh
130-131. Central Research Library
132-151. Laboratory Records Department
152. Laboratory Records, ORNL-RC
153-154. ORNL Y-12 Technical Library Document Reference Section
155. Reactor Division Library, Bldg. 9204-1, Y-12

EXTERNAL DISTRIBUTION

156. Division of Research and Development, AEC, ORO
157-665. Given distribution as shown in TID-4500 (15th ed.) under Reactors-General category